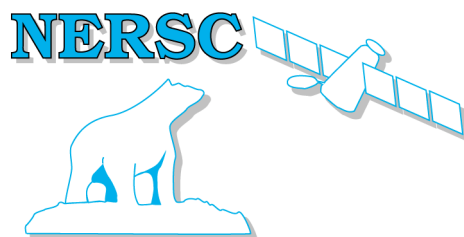


Nansen Environmental and Remote Sensing Center

*A non-profit
Research institute affiliated
With the University of
Bergen*



*Thormøhlensgate 47
N-5006 Bergen,
Norway
<http://www.nersc.no>*

NERSC Technical Report no. 267

Sea ice modelling and remote sensing in the Barents and Kara Sea

Part B: Remote Sensing



Photograph of an iceberg drifting in sea ice. Courtesy: A. Glazovsky



Project for Statoil ASA in 2005

Statoil Order no. 4500909324

Authors:

*Stein Sandven, Laurent Bertino, Knut Arild Lisæter, Intissar Keghouche, Hanne Sagen,
Kjell Kloster, and Mohamed Babiker*

January 2006

  <p>Mohn-Sverdrup Center Global Ocean Studies - Operational Oceanography</p>	<p>Nansen Environmental and Remote Sensing Center (NERSC)</p> <p>Thormøhlensgate 47 N-5006 Bergen, Norway Phone: + 47 55 20 58 00 Fax: + 47 55 20 58 01 E-Mail: Stein.Sandven@nersc.no http://www.nersc.no</p>
--	---

<p>TITLE:</p> <p>Sea ice modeling and remote sensing in the Barents and Kara Seas</p> <p>Part B: Remote Sensing</p>	<p>REPORT IDENTIFICATION</p> <p>NERSC Technical report no. 267</p>
<p>CLIENT</p> <p>STATOIL ASA</p>	<p>CONTRACT</p> <p>Order no. 4500909324</p>
<p>CLIENT REFERENCE</p> <p>Einar Nygaard</p>	<p>AVAILABILITY</p> <p>Customer report</p>
<p>INVESTIGATORS</p> <p>Stein Sandven, Laurent Bertino, Knut Arild Lisæter, Intissar Kéghouche, Hanne Sagen, Kjell Kloster, and Mohamed Babiker</p>	<p>AUTHORISATION</p> <p>Bergen, 20 January 2006</p> <p>Stein Sandven</p>

Contents

EXECUTIVE SUMMARY	2
1. OVERVIEW OF THE ICE SEASON 2005	3
2. USE OF SAR IMAGES FOR ICE NAVIGATION IN THE NORTHERN SEA ROUTE.	9
2.1 BACKGROUND	9
2.2 INTRODUCING ENVISAT ASAR WIDESWATH IMAGES	9
2.3 EXPERIENCE FROM THE SAR ICE MONITORING IN 2004	10
2.4 SAR ICE MONITORING IN 2005.....	12
3. SEA ICE SIGNATURES IN SAR IMAGES	19
3.1 NEW ICE.....	19
3.2 YOUNG ICE	20
3.3 FIRST YEAR ICE	21
3.4 MULTIYEAR ICE	23
4. USE OF OPTICAL SATELLITE IMAGES	25
4.1 MODIS IMAGES.....	25
4.2 LANDSAT IMAGES	27
4.3 COMPARISON OF SAR AND LANDSAT IMAGES.....	29
4.4 ASTER IMAGES FOR ICEBERG DETECTION	30
5. ICE ROUGHNESS AND THICKNESS FROM ICESAT.....	33
5.1 TECHNICAL INTRODUCTION	33
5.2 EXAMPLES OF LASER PROFILE DATA	33
6. CONCLUSIONS AND RECOMMENDATION FOR FURTHER WORK.....	37
7. REFERENCES.....	38

Executive Summary

Part A of this report describes the ice-ocean modeling work carried out in the Arctic Ocean and with focus on the Barents Sea & Kara Sea area under the contract between the Nansen Center and Statoil for 2005. The main activity has been to set up and run test simulations with the high resolution coupled sea ice – ocean model with about 5 km resolution (the Barents Sea model). The Barents Sea model is nested with the large-scale TOPAZ system covering the whole North Atlantic and Arctic. Like the TOPAZ system, the Barents Sea model is based on the HYCOM ocean model and uses Elastic Visco Plastic (EVP) rheology for the sea ice model. The atmospheric forcing fields are from European Centre for Medium-Range Weather Forecasts (ECMWF).

The Barents Sea model have been run for four months in 1979, which was a heavy ice year, and validated with respect to water mass fluxes, temperature and salinity fields and ice edge/ice concentration. An iceberg model have been obtained from Alfred Wegener Institute and will be coupled to the Barents Sea model in 2006. From these components an iceberg drift forecasting model will be implemented and validated.

Ice thickness simulations from the North Atlantic model, run for the period 1958 – 2002, have obtained and validated for the Arctic Basin. Ice thickness statistics in selected parts of the Barents Sea have been estimated. The Barents Sea model including the iceberg model will be further tested and validated in 2006. The objective is to establish an operational forecasting system for icebergs, sea ice drift and currents by 2007.

Part B described the satellite remote sensing activities performed in the Statoil contract for 2005. We have collected and analysed several types of satellite data that can quantify some of the sea ice and iceberg properties that are important for planning of Statoil's activities in the Barents and Kara Sea region. Daily passive microwave data are useful for mapping ice concentration and ice extent on regional scale in order to follow the ice edge and ice drift. These parameters are needed as input data in sea ice and iceberg drift models. At present daily, near real-time data are assimilated in the TOPAZ ice forecasting model, and will be used also in the Barents Sea model.

For detailed mapping of ice types, ice concentration, ice drift, ice convergence/divergence, multiyear floes, ridges and leads SAR images have been collected for most of the study period in 2005. Several examples of analysis of the SAR images, including ice drift retrieval, have been shown. From February SAR widesswath mosaics have been made more or less regularly throughout the year in the Barents/Kara Sea region. This demonstrates how ice mapping can be improved compared to the standard ice charts delivered by the national ice services. 2005 is the first year when such SAR mosaics are produced in the Barents/Kara Sea region. SAR is the most important space instrument for mapping sea ice properties in support of ice operations and navigation.

For iceberg detection, high resolution optical images have been demonstrated in the Franz Josef Land area. In one ASTER image more that 100 icebergs were found embedded in the fastice surrounding the archipelago in May 2005. For monitoring of iceberg production and iceberg drift, it is useful to have a systematic scheme for optical as well as SAR images with sufficient high resolution. Use of satellite altimeter data for ice surface topography, ridges and thickness mapping has been investigated with examples of IceSat data from 2003.

Finally, recommendations for further work are indicated in both part A and B.

1. Overview of the ice season 2005

An overview of the ice season 2005 in the Barents and Kara Sea is presented in this chapter. The main source of information is passive microwave satellite data from the AMSRE system (Advanced Microwave Scanning Radiometer on EOS). Institute of Environmental Physics at University of Bremen provides near real time worldwide sea ice maps from this satellite. The ice concentration product is based on the 89 GHz data of AMSR-E with a spatial resolution of 5x5 km. New ice maps are produced every day. More information about the AMSR-E and other ice products is found on <http://www.seaice.de>. Ice concentration maps from the SSMI sensor, which are available since 1978, are available at the Nansen Center server: <http://www.nersc.no/Seaice/>. Two ice charts per month from the AMSR-E data are presented in Figs 1 – 4, starting in February and continuing until the end of December 2005.

The winter 2005 was characterised as a light ice year in the Barents Sea. The eastern Barents Sea had little ice, mainly in the Pechora Sea and around Kolguyev Island. The Shtockman field had hardly any ice at all. Maximum ice extent in this area was from late March to mid April. The melting with retreat of the ice edge started in early May. By the end of May, the Pechora Sea was ice-free while the Kara Sea was still fully ice-covered. The melting and retreat of the ice in the Kara Sea started in June and lasted till the end of July. In August and September the ice edge continued to retreat north of 80 N. The minimum ice extent occurred in the second half of September. At that time the whole Northern Sea Route was ice-free. Vessel could sail in open water north of all the Russian Islands (Novaya Zemlya, Severnaya Zemlya, Siberian Islands and Wrangel Island). This is a much shorter route between the Barents Sea and the Bering Strait compared to coastal route along the Siberian coast. The record low ice extent is associated with the very warm year in the Arctic, where the air temperature in the European sector of the Arctic was up to 4 deg C above normal (Fig. 5 a). The ice extent is also governed by the ocean temperature and salinity. The minimum ice extent for the last four summers are (shown in Fig. 5 b) are well below the average over the last 22 years.

Refreezing started in October and the Laptev Sea and the northern part of the Kara Sea were quickly covered with thin and young ice, typically up to 30 cm thick. During November and December the ice edge was practically stationary at 78 N. The whole Barents Sea south of 78 N was still ice-free by 01 January 2006. The southern Kara Sea was freezing very slowly in the period.

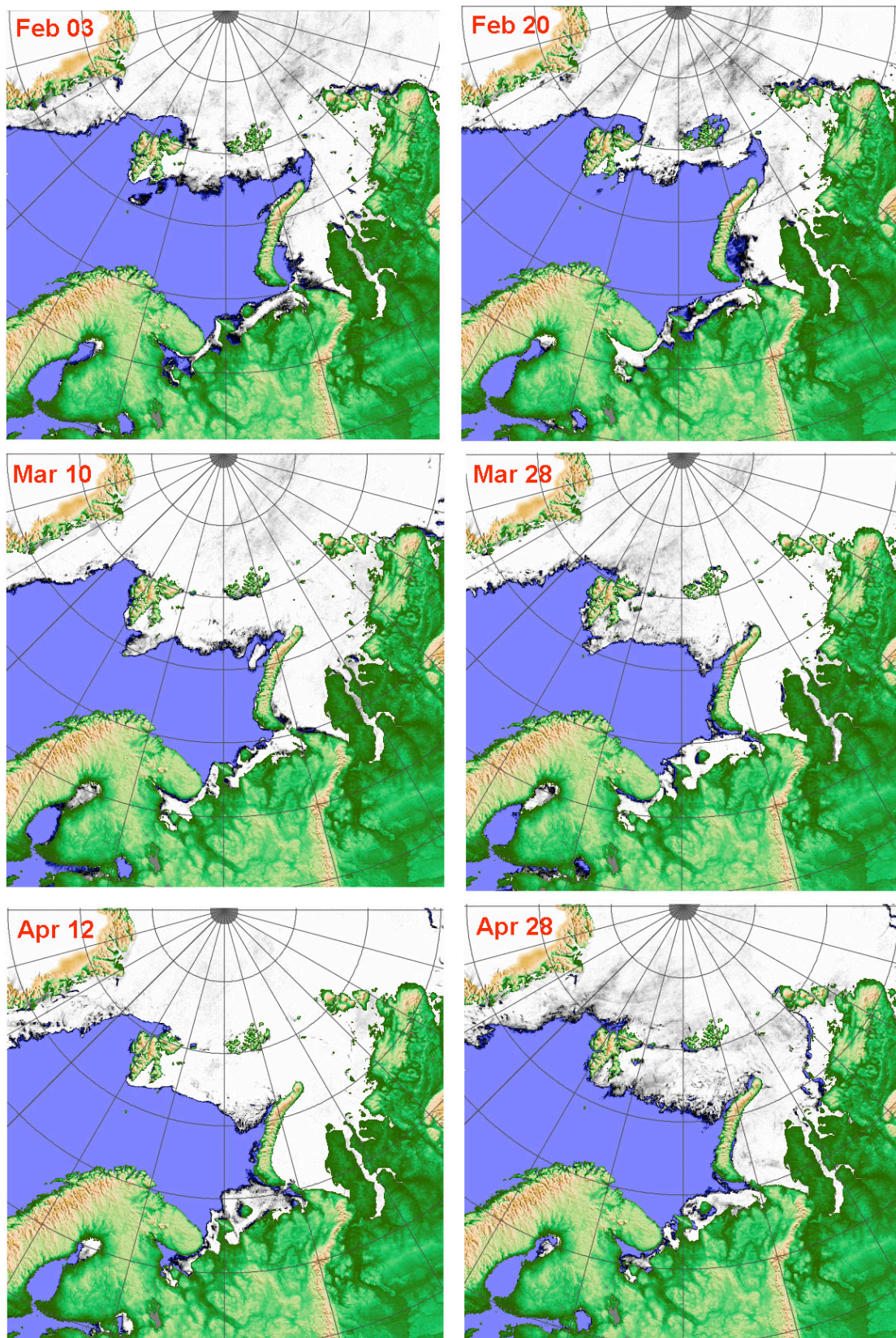


Figure 1. Ice charts from AMSR-E data for February – April 2005. Courtesy Univ. of Bremen.

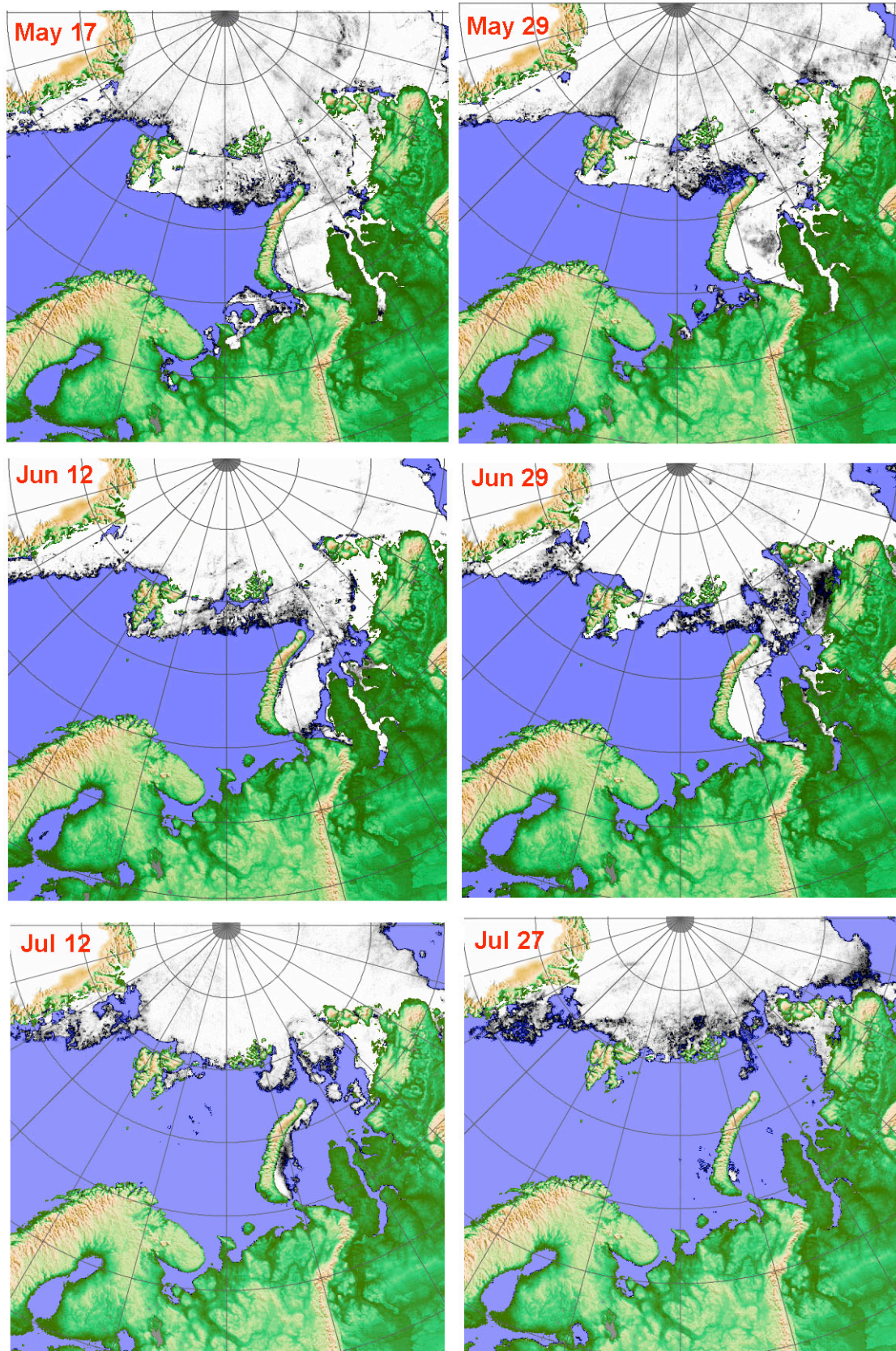


Figure 2. Ice charts from AMSR-E data for May – July 2005. Courtesy Univ. of Bremen.

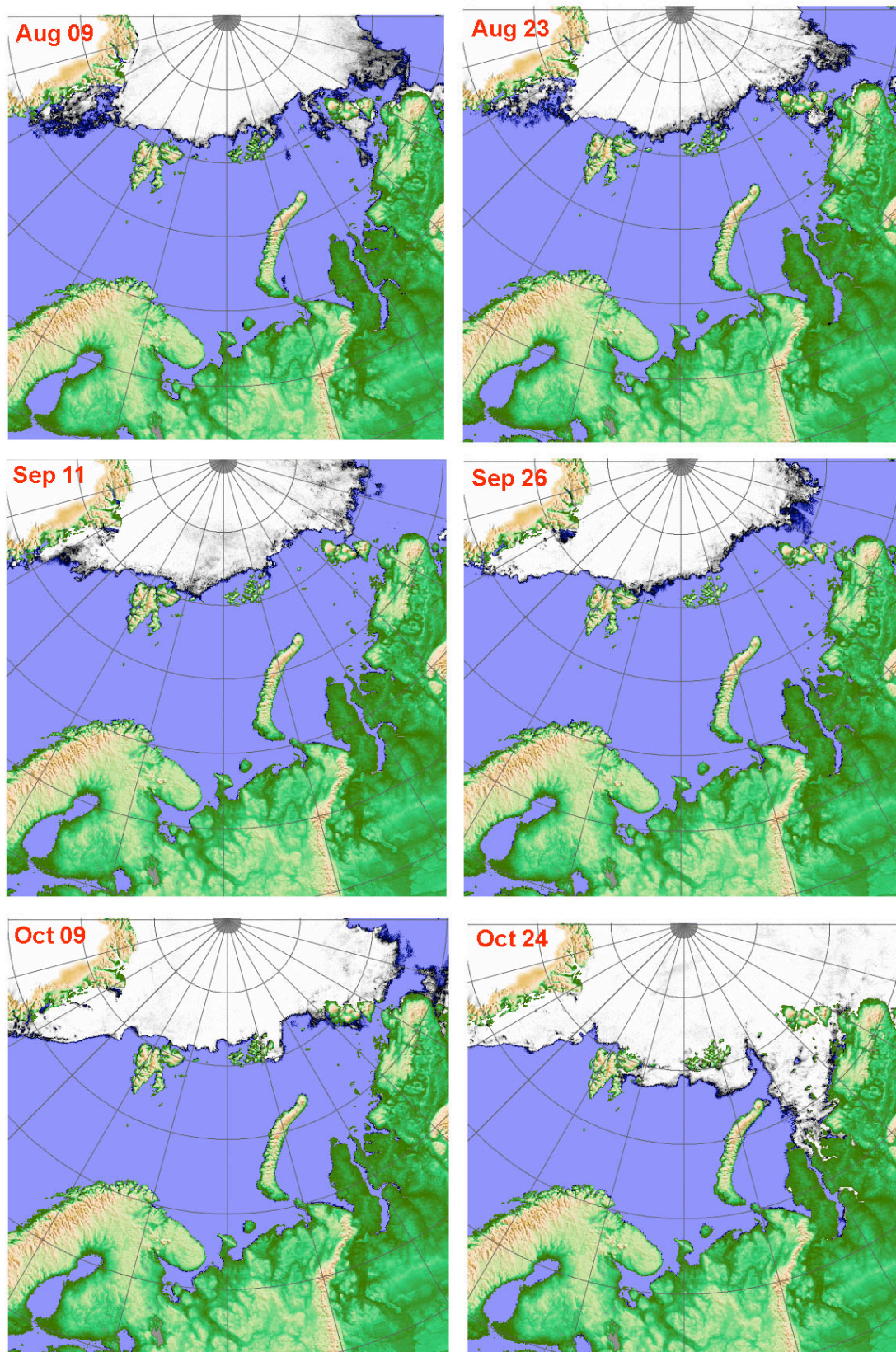


Figure 3. Ice charts from AMSR-E data for August – October 2005. Courtesy Univ. of Bremen.

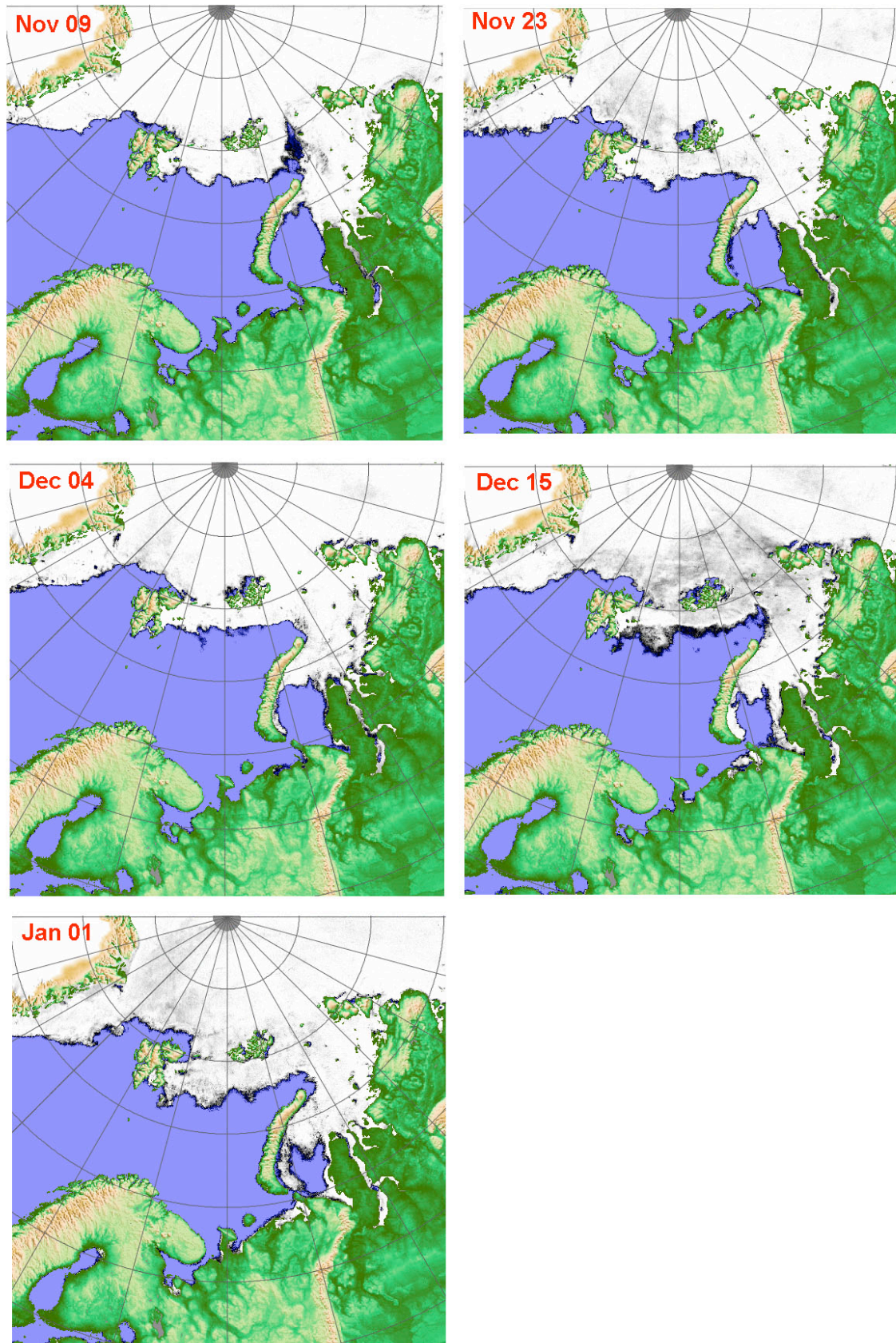
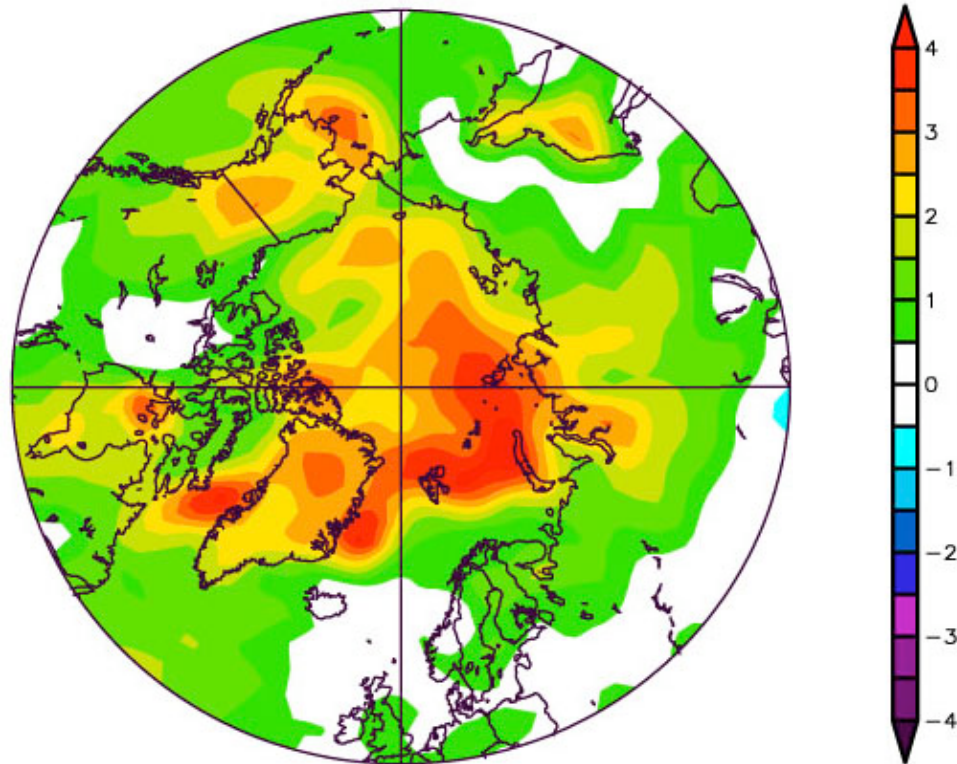
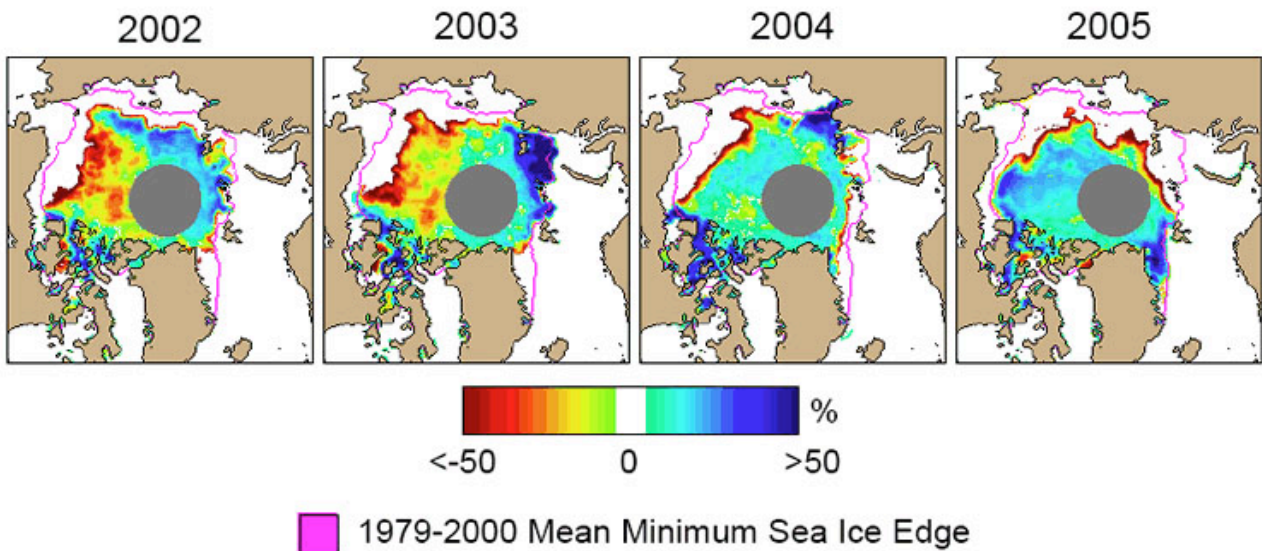


Figure 4. Ice charts from AMSR-E data for November – December 2005. Courtesy Univ. of Bremen.



a



b

Figure 5. a) Surface air temperature anomaly in the Arctic for January – August 2005. The European sector of the Arctic had about 4 deg C above normal. b) The minimum ice extent showed a record minimum in September 2005. The four last summer minima (2002 – 2005) were all well below the average minimum, indicated by the pink line. The colour code indicates the ice concentration anomaly compared to the average over the last 22 years.

2. Use of SAR images for ice navigation in the Northern Sea Route.

2.1 Background

Use of satellite SAR data for sea ice monitoring in the Northern Sea Route was initiated in August 1991, when the first ERS-1 SAR images were obtained, analyzed and transmitted onboard the French vessel L'Astrolabe during her voyage from Europe to Japan. In 1993 Nansen Centres in Bergen and St. Petersburg together with Murmansk Shipping Company started extensive campaigns to demonstrate use of SAR data for supporting icebreaker navigation in ice. During the 1993/1994-winter season several hundreds of ERS-1 SAR images were transmitted to the Marine Operational Headquarters and to the nuclear icebreakers operating along the Siberian coast (Fig. 6). These campaigns demonstrated that SAR data can enhance significantly the quality of sea ice monitoring, although the spatial coverage of ERS-1 SAR images the Northern Sea Route was limited. In 1996 the ESA¹ and the Russian Space Agency initiated the cooperative ICEWATCH Project, aimed at utilizing various remote sensing data for sea ice monitoring. In this project the use of SAR data onboard the icebreakers were continued (Johannessen et al., 1996, 1997, 2000, 2005). The RADARSAT ScanSAR improved the possibility of mapping larger areas of sea ice compared to ERS due to the swath width of up to 500 km. The demonstration conducted onboard the icebreaker Sovetsky Soyuz in summer 1997 showed that the most important sea ice parameters could be derived from these images during summer conditions (Sandven et al., 2001). ScanSAR data were found particularly important for supporting icebreaker operations during the winter 1997/1998 between Murmansk and the Yenisey River, where year-round ship navigation is performed by Murmansk Shipping Company (Alexandrov et al., 2000, Pettersson et al., 1999).

2.2 Introducing ENVISAT ASAR wid swath images

The first use of ENVISAT ASAR data for ice navigation in the Northern Sea Route was demonstrated onboard the icebreaker *Sovetsky Soyuz* in the summer of 2003. The summer ice conditions in the Kara Sea are usually light and do not cause any problems for the icebreakers. The purpose of the demonstration was therefore to test technical feasibility of ordering, producing and transmitting wid swath images to the icebreakers in near real time. In winter and spring of 2004 and 2005 wid swath SAR images were ordered based on recommendations from Murmansk Shipping Company which operates the icebreakers in the regions. After receiving full-resolution ASAR images from ESA or KSAT², geolocation, antenna correction and image compression, the images were sent to the Marine Operation Headquarter (MOH) of Murmansk Shipping Company. The resolution of the images was 600 m/pixel and the images were transmitted by e-mail to MOH as jpg-files. Using these data MOH planned the routes of convoys in the sea ice of the Barents and Kara Seas, including the Ob and Yenisey gulfs. From MOH the images and the results of analysis were transmitted to the nuclear icebreakers *Yamal*, *Sovetsky Soyuz*, *Arktika*, *Vaygach*, and *Taymyr* via the TV channels of the "Orbita" systems. This system is used for communication and data transmission to all the MOH icebreakers.

SAR images from ENVISAT Wid swath data (pixel size 150 m) provide detailed information about ice conditions (ice edge, ice types, polynyas, leads, fast ice, drifting ice, and rough ice versus level ice). Systematic mapping by SAR can therefore provide much better quality of the ice monitoring compared to other methods, although the coverage of the SAR data is not sufficient to map all the required sea ice areas. SAR data from ENVISAT are available in the Barents and Kara

¹ European Space Agency, operator of the ERS and ENVISAT programmes

² Kongsberg Satellite Services, producer of SAR images in the European sector of the Arctic

Sea region through various research projects at NERSC. The SAR images are primarily used to map ice features of importance for ice navigation and other ice operations. During 2005 a number of SAR images, shown in section 2.4, have been transmitted to Murmansk Shipping Company and used by the operational headquarter to plan navigation of the Russian nuclear ice breakers in the western part of the Northern Sea Route (Fig. 6). Retrieval of various ice parameters of importance for navigation is demonstrated, in particular leads, ridges, convergence zones and areas of ridged ice and multiyear ice. As supplement to SAR images, examples of high-resolution optical images are presented, and the possibility to retrieve ice parameters is demonstrated.

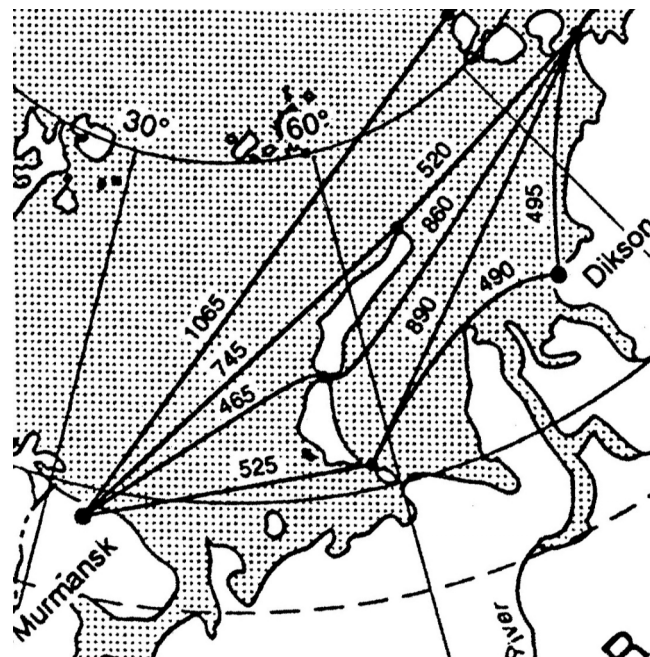


Figure 6. The main alternative sailing routes between Murmansk, Dikson (Yenisei River) and areas further east. The numbers indicate sailing distances in nautical miles (Mulherin, 1996).

2.3 Experience from the SAR ice monitoring in 2004

From February 2004 ASAR images were used for support of the icebreaker convoys, which in that period were steered along the coast through the Kara Gate, to Belyi Island and then to Dikson, passing to the south of $74^{\circ} 30'N - 75^{\circ}N$. This is the southernmost route shown in Fig. 6. The analysis of the ASAR images for early February showed vast areas of open water south of Novaya Zemlya, reaching up to the eastern entrance to the Kara Gate as well as very close ice in the southwestern part of the Kara Sea. Using this information the convoy's formation place in open water and its sailing route were determined. The possibility of ship entering into the fast ice within the accessible depths was assessed in the Cape Kharasavey area, located on the west coasts of the Yamal peninsula.

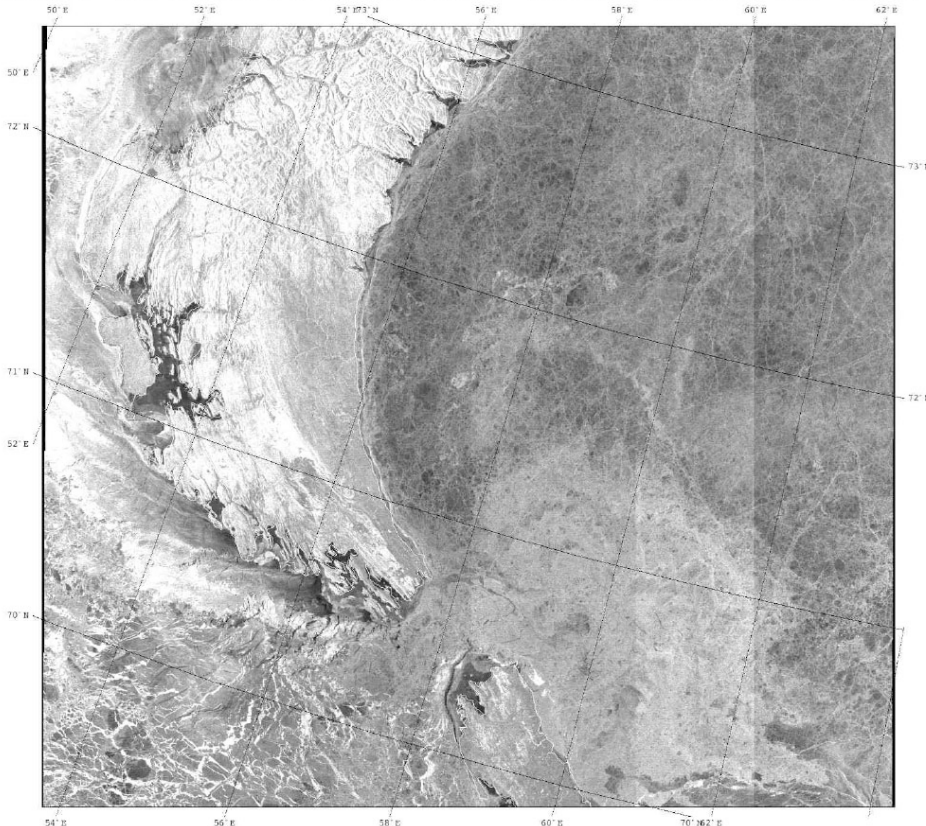
The central part of the Kara Sea including the Yenisei Gulf was covered with a series of ASAR images from 14 February (Fig. 7, 8) to 07 May. The images were used to determine the fast ice boundary and areas of various degrees of deformation. Thin first-year ice located north of fast ice is clearly evident. ASAR-derived ice information was transmitted to the icebreakers *Arktika* and *Sovetsky Soyuz*, steering convoys from the west to Dikson, and to the icebreaker *Taymyr*, sailing from Dudinka up to the Yenisey. Another image for February 18, covering the westernmost part of the NSR (Fig. 7b), shows heavily ridged sea along the eastern approach to the Kara Gate Strait, which made navigation along the coastal route problematic.

ASAR 14.Feb.04 16:00z Kara Sea for MSC.



Figure 7. a) ASAR wide-swath image of the central Kara Sea obtained on 14 February 2004. The Yamal peninsula is seen in the lower left part and the Yenisei Gulf in the lower right part of the image. Note the dark signatures in the image indicating nilas and grey ice along the coast but outside the fast ice areas.

ASAR 18.Feb.04 17:15z Kara Sea for MSC.



b) ASAR wide-swath image of the western Kara Sea, the Kara gate and the Pechora Sea obtained on 18 February 2004. Note the bright signature of the rough first-year ice which has drifted eastwards through the Kara gate and into the Kara Sea. The Pechora Sea shows less compact ice with many leads characterized by bright signature.

The area west of Novaya Zemlya showed mainly young ice and open water. In such cases the sailing route north of Novaya Zemlya is often used by the icebreakers to avoid the Kara Gate. The central Kara Sea is covered by first-year ice with less roughness compared to the rough ice which has drifted through the Kara Gate. The wide flaw polynya in the Ob-Yenisey region, covered with the young ice, is clearly seen in the ASAR image of February 24 (Fig. 8 a). A convoy sailed along it to Dikson without any problems. The next image of March 11 (not shown here), shows that first-year ice moved northward during these days and young ice prevail to the south of 75°N. Later ASAR images confirmed that grey-white ice and thin first-year ice prevail in the Ob-Yenisey region. The ASAR images of the Yenisey Gulf allow discrimination between level and deformed fast ice. It was found that level ice without ridges was located along its eastern coast, and a new channel was made in it. The icebreaker navigators received the ASAR images and interpreted them in order to select the best sailing routes, which included level thin ice, leads and polynyas. Also avoiding large ice floes was important. As a result the average speed of convoys in the ice increased up to 40-60%.

The acquisition of *ENVISAT* images and their delivery to MSC was continued until June 2004 when the ice started to disappear in the sailing routes. The images documented changes of ice conditions during the period of summer melting. On June 17 with the advance of melting only open water and very open ice are evident seaward of the fast ice boundary in the Ob-Yenisey region, thus making the navigation along the coastal route easy. The image of June 24 (Fig. 8 b) shows open water in all this area and very open ice further to the north. The fast ice boundary, which can be easily detected in this image, did not change appreciably, except of the Yenisey Gulf, where it was broken-up by the icebreakers. Large pieces of the fast ice can be seen near Dikson.

2.4 SAR ice monitoring in 2005

In the winter of 2005 the sea ice conditions in the Kara Sea did not limit the navigation along the shortest coastal route until the end of February. Analysis of images for February 12-13 showed that the ice massif had shifted from Novaya Zemlya toward the northeast and formed an area of strong compaction near the western coast of Yamal peninsula and Belyi Island. Therefore, MOH selected a new sailing route passing from the Kara Gate along the fractures to Dikson. The first mosaic was produced from several ASAR stripes for the period February 26-28. This mosaic, with the sailing route superimposed, is shown in Figure 9 a. Analysis of the ASAR images together with the sea ice observations shows that young ice covered vast areas east of Novaya Zemlya (area 1 in Figure 9a). Moderately deformed thin first-year ice prevailed to the east of approximately 67°E (area 2). A number of fractures, stretching in the northeastern direction, is clearly seen (area 3). Due to the use of ASAR images the average speed of convoys in the ice increased up to 40% in February.

In late March sea ice conditions became unfavorable in the central part of the Kara Sea, where the ice massif blocked the route north of Belyi and Vilkitsky Islands. As a result the average speed of convoys in this period decreased to 9.7 knots from 11 knots in early March. This route with minor variations was still used in early April, and *Sovetsky Soyuz* together with *Vaygach* escorted *Noril'sk* to the Pechora Sea. However, based on available *NOAA* images it was decided to navigate around Cape Zhelaniya, and ice conditions there were described from the ASAR images. In the second part of April, the convoys sailed from Dikson to Arctic Institute Islands and Izvestiy TSIK Islands, where easterly winds formed wide polynyas, and from here to Cape Zhelaniya across relatively level ice. Along wide flaw polynyas west of Cape Zhelaniya ships could navigate without the icebreaker support.

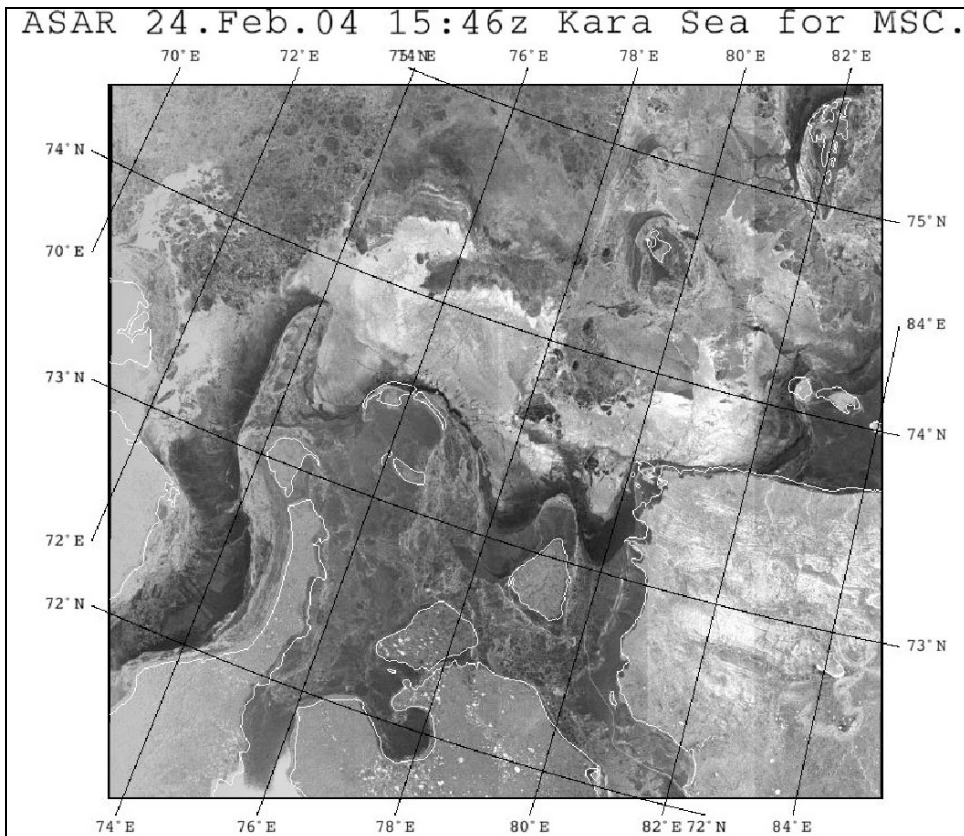


Figure 8a. ASAR wide-swath image of the central Kara Sea obtained on 24 February 2004. Note the bright signature of the young ice in the flaw polynya from Belyi island in west to the area of Dikson in east.

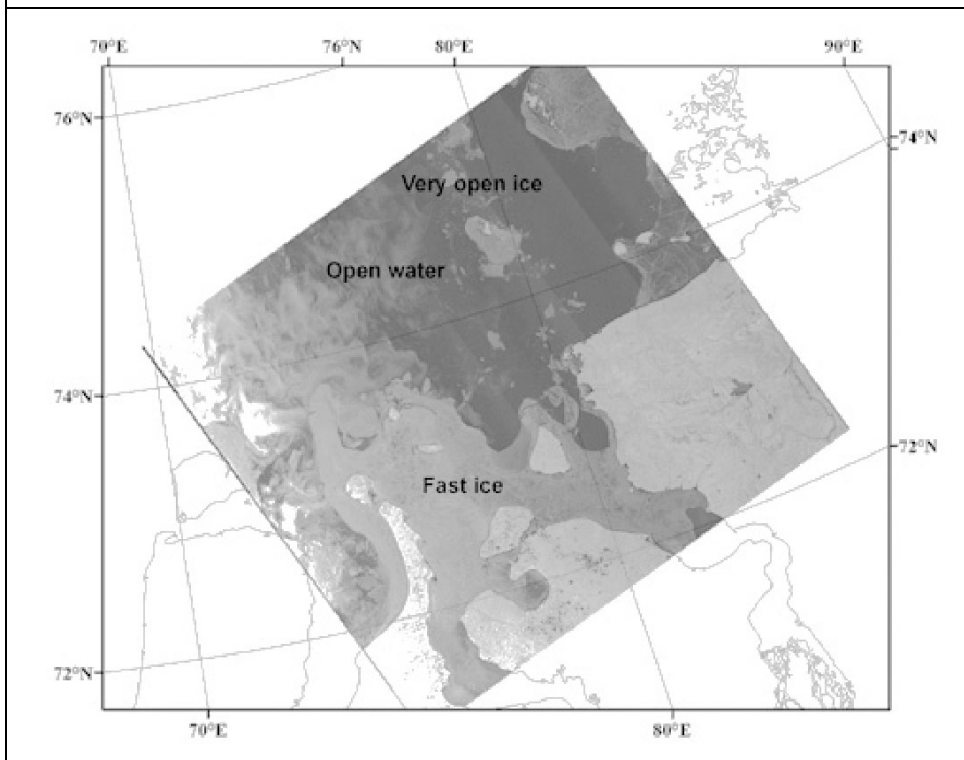


Figure 8b. ASAR wide-swath image of the central Kara Sea obtained on 24 June 2004 when ice melting is in progress. Note the bright signature of the fast ice while open water has signature varying from dark to bright depending on the wind speed.

Thus on April 27–29, the icebreaker *Arktika* escorted *Kandalaksha* from Dikson to the ice edge in the Barents Sea. The average speed of ships in ice increased in April by up to 41%, as compared with average speed for this type of sea ice conditions. During May convoys also sailed along this route. Thus, the icebreakers *Arktika*, *Yamal*, and *Vaygach* steered *Sevmorput*, *Noril'sk* and *Kola*

from Dikson to the Barents Sea during May 22 – 25. Their route overlaid on mosaic of ASAR images is shown in Figure 9b.

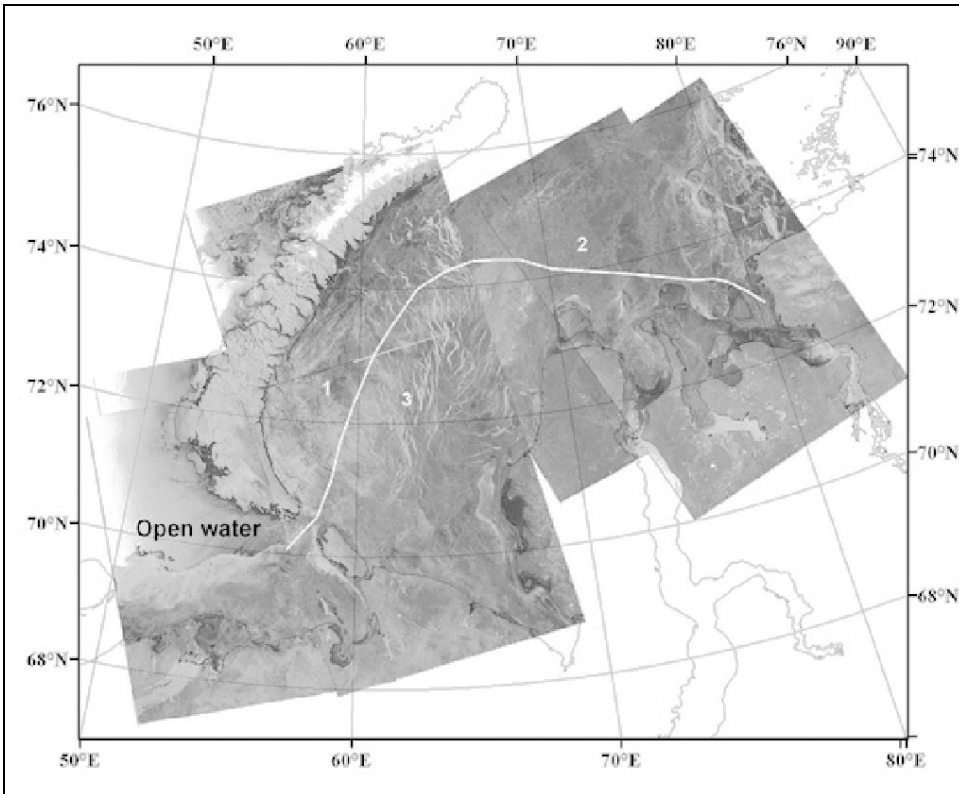


Figure 9a. Mosaic of four ASAR widewath stripes obtained 26 – 28 February 2005. The sailing route of the convoy between Kara gate and Yenisei Gulf is superimposed

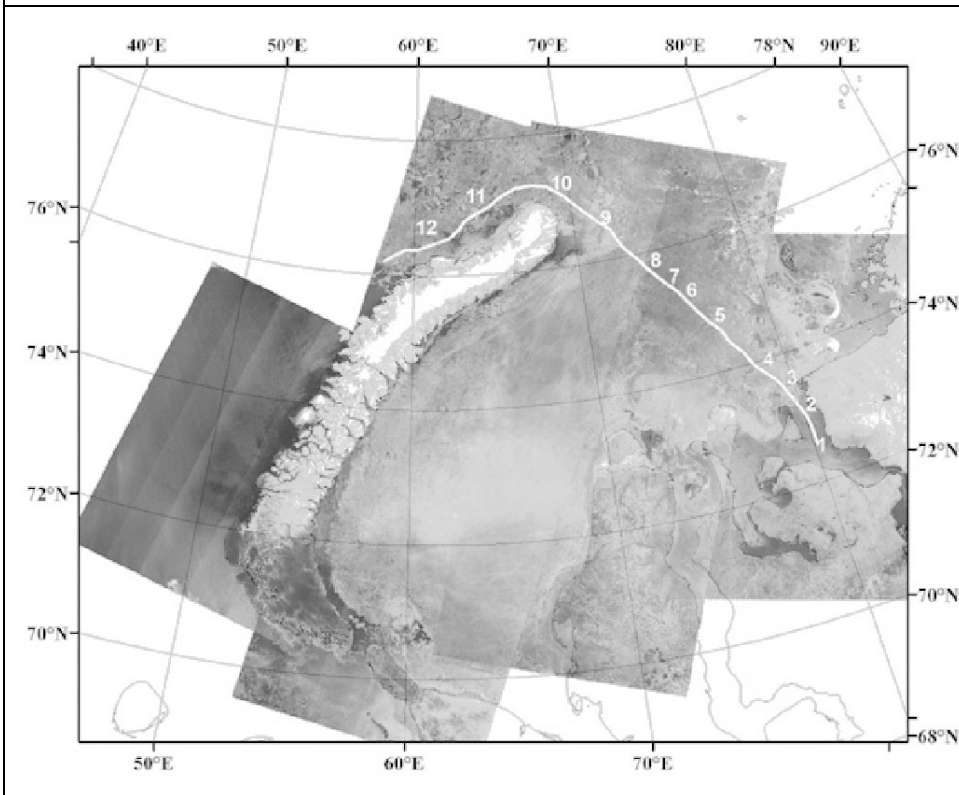


Figure 9b. Mosaic of four ASAR widewath stripes obtained 21-24 May 2005. The sailing route of the MSC convoys between Yenisei Gulf and Barents Sea, which goes north of Cape Chelania, the northern tip of Novaya Zemlya, is superimposed on the mosaic.

The radar signatures along the sailing route were compared with ship observations of sea ice. Thick first-year fast ice in the Yenisey Gulf (point 1) has a dark tone, and its boundary is clearly visible in the image. With the beginning of snow melting and increased moisture of the surface the rough fast ice is difficult to distinguish from level ice. The drifting ice between points 2 and 5 has brighter signature than the fast ice and the drifting ice further northward. It corresponds to close ice, consisting of thin first-year and young ice. Further north (points 6-10) generally darker image tone corresponds to very close ice. Here the first-year ice prevails, and variations of SAR signature from dark to slightly bright are probably caused by differences in surface roughness due to ridging and ice floe size. Thus, ice breccia and small floes of medium first-year ice, observed at point 9, are shown with brighter tone in the image. Westward of Novaya Zemlya (points 11 and 12) ice concentration decreases, and some open water areas can be detected in the ASAR image.

The use of ASAR images during May resulted in an increase of the average ship speed in ice by up to 46%. Also in the period 14-16 May, the icebreaker *Yamal* accomplished the operation on breaking-up of the fast ice in the Yenisey Gulf using a combination of traverses, determined from the ASAR images. The icebreaker *Taymyr* continued this work on May 23-26.

The sea ice conditions in the Kara Sea during the winter-spring of 2005 were easier than average long-term conditions. This circumstance decreased to some degree the efficiency of using the ASAR images, but even then the average speed of ships in ice increased by about 30-40%, as compared with the normal values for the given type of ice conditions.

ENVISAT ASAR have produced from 5 to 10 images stripes per week over the eastern Barents Sea and Kara Sea during 2005. Examples of these stripes are shown, where stripes obtained during a 2 – 3 day period are merged into mosaics. The mosaics will therefore give a near synoptic picture of the ice conditions (Fig 9). Example of ice charts produced from SAR mosaics is shown, where the main ice classes showing the stage of development (SOD) are identified (Fig. 10). Ice charts from SAR are more detailed and accurate than the standard ice charts produced by the Russian ice service in this region. By comparing features between consecutive mosaics, the ice motion can be retrieved.

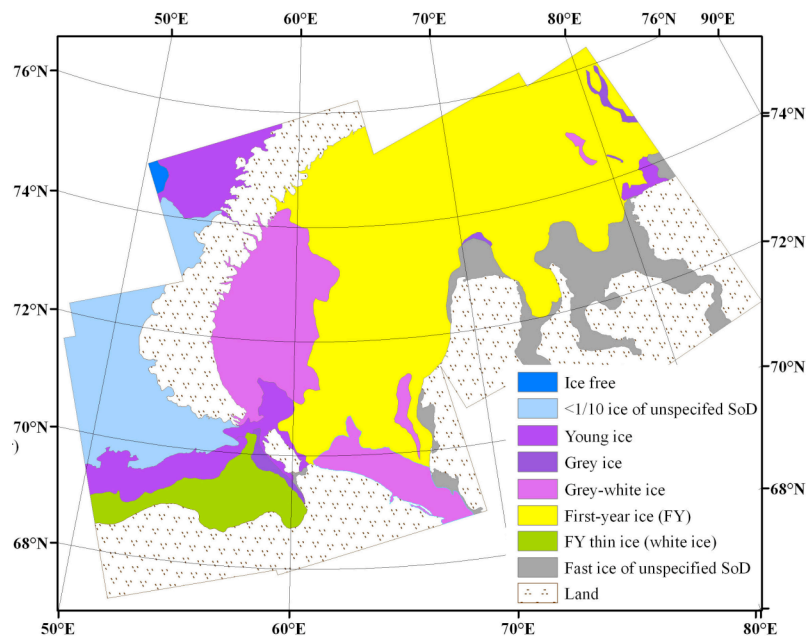


Figure 10. Example of ice chart derived from the SAR mosaic 27 – 28 February 2005, where the stage of development of ice types is shown.

Further examples of ASAR mosaics from 2005 are shown in Figures 11 and 12. These examples include ice drift vectors showing the displacement of ice features such as floes, leads and ice edges over 2 – 3 days.

Ice drift data will be important for the validation of the Barents Sea model. From sequential SAR mosaics, it is feasible to retrieve quite detailed information about the ice drift. The main limitation of the SAR data is lack of systematic data coverage every day. For large scale mapping of ice drift there are operational products from satellite scatterometer provided by Ifremer. Examples of a scatterometer ice drift products in the Barents and Kara Sea are shown in Fig. 13. A single ice drift map covering the period 14 – 16 April 2004 is shown in Fig. 13a. This illustrate that the scatterometer has too coarse resolution to retrieve ice drift in areas such as the southeastern Barents Sea and southern Kara Sea. By combining continuous ice drift vectors for a whole winter season, it is possible to estimate drift trajectories, as shown in Fig. 13 b. Such trajectories are useful for model validation and to assess the seasonal ice drift. SAR ice drift vectors are more detailed and can be retrieved near coasts. An example of ice drift with 3 day interval in late May 2005 in the Kara Sea is shown in Fig. 13c. Systematic acquisition of SAR data in the Barents and Kara Sea makes it possible to estimate the ice drift much more accurately than from other satellite systems.

ASAR 16.-18.Jun.2005 Mosaic of WP 600m/p

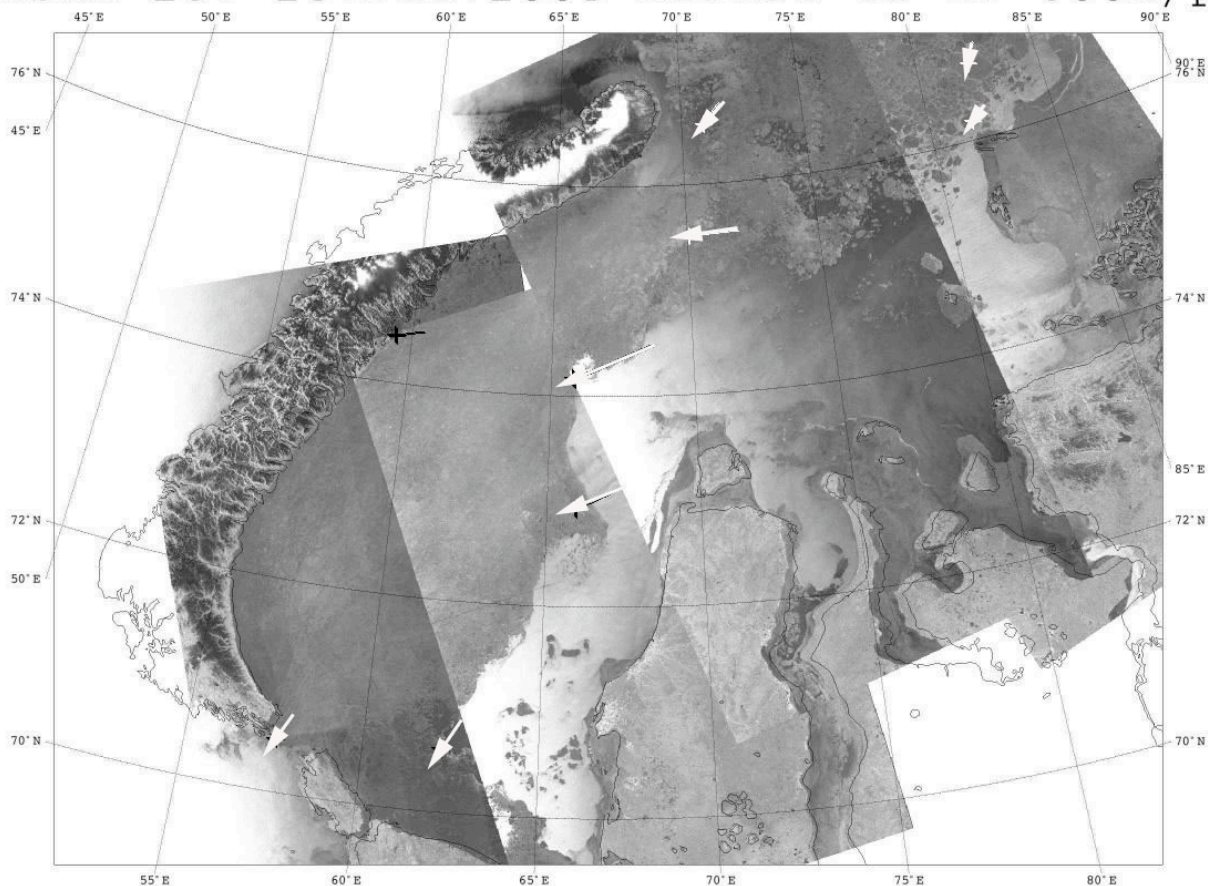


Figure 11. Mosaic of SAR stripes showing ice extent and ice drift in the period 16 – 18 June 2005. This was the last mosaic from the Kara Sea in the melt season before the ice edge retreated further north in July – August.

ASAR 14.-16.Dec.2005 w/3-days ice-displ.

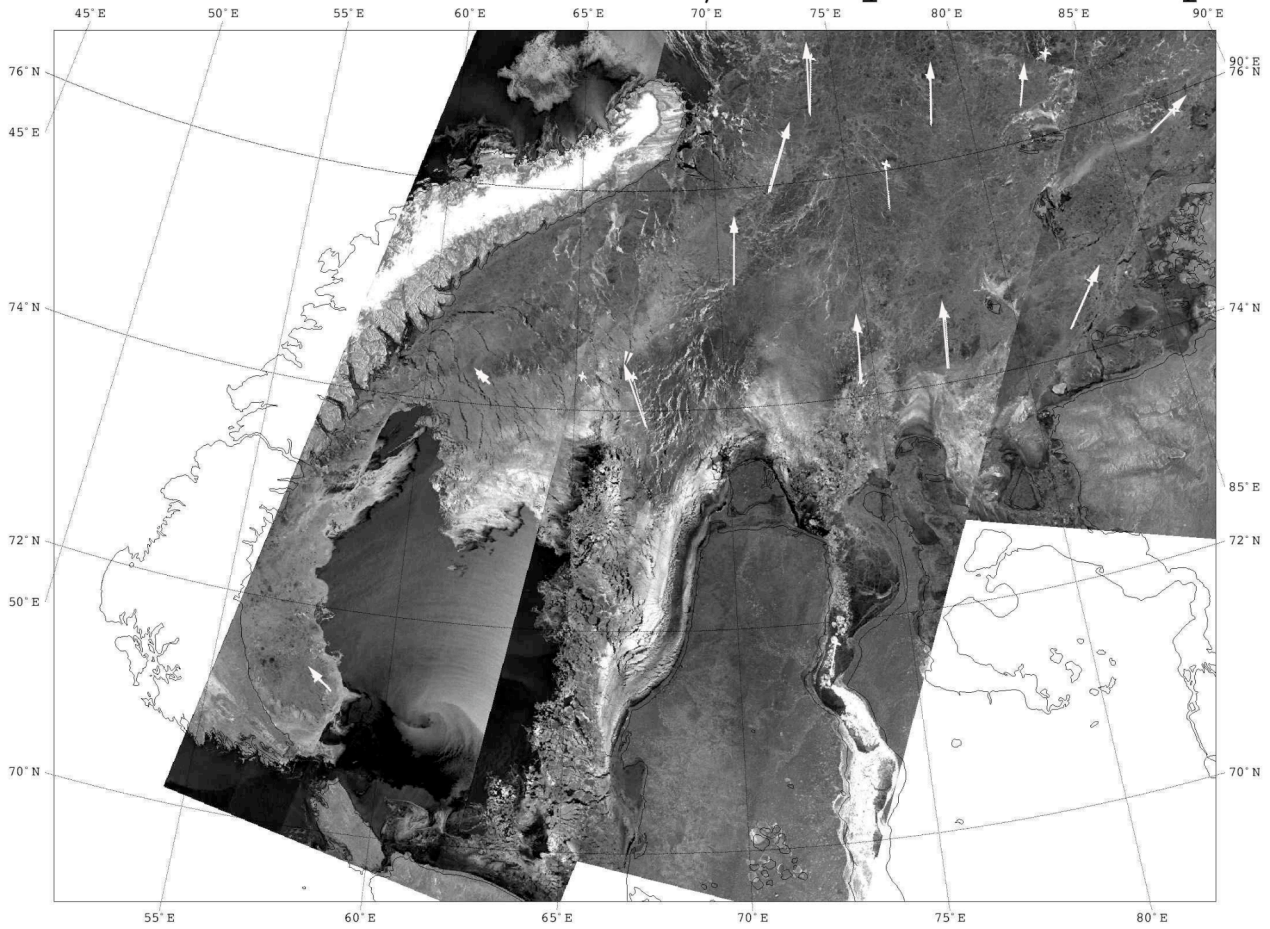


Figure 12. ASAR mosaic and ice drift vectors for the period 14 – 16 December 2005. This the period of refreezing in the Kara Sea.

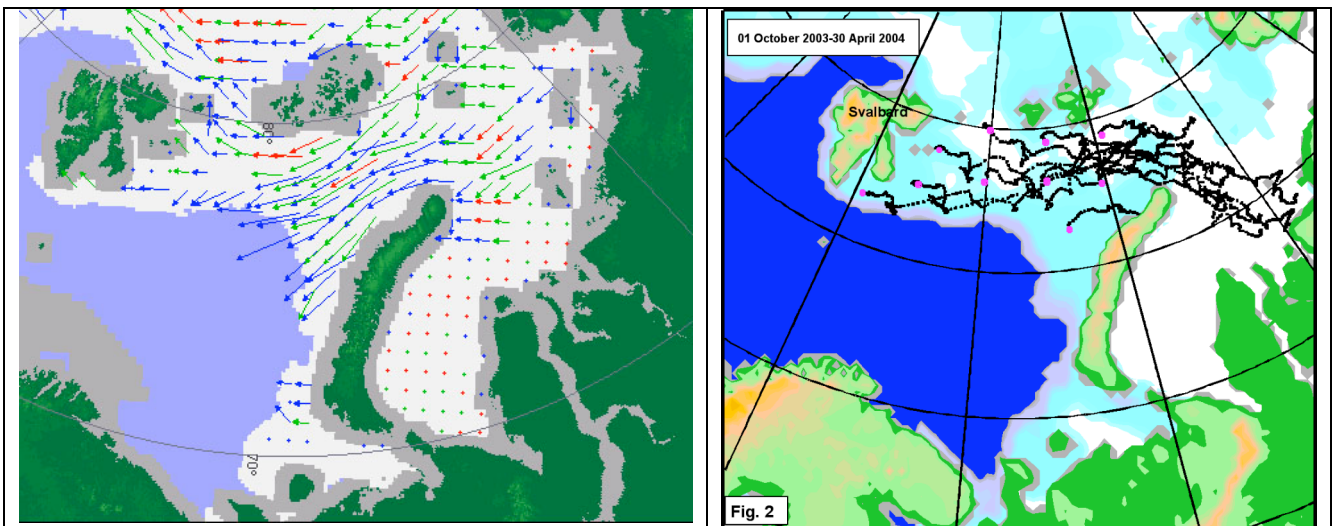
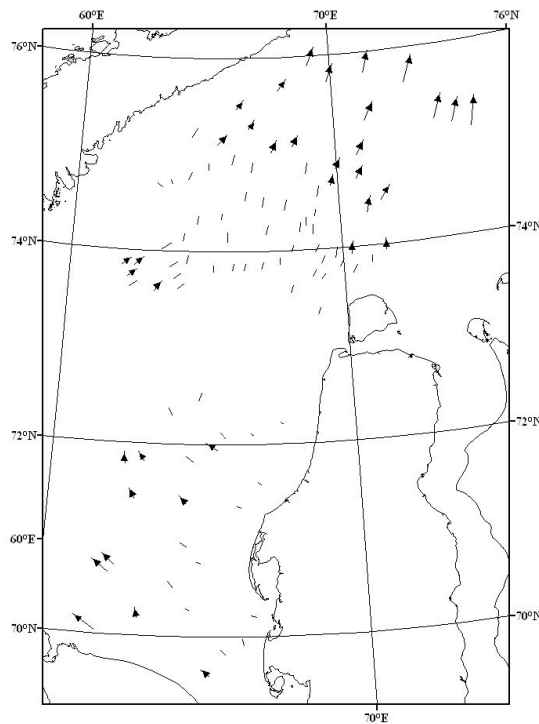


Figure 13 . Ice drift from scatterometer data: a) ice drift map 14 – 16 April 2004 (ref. Ifremer); b) ice drift trajectories for the winter season 2003-04 (ref. NPI). Note that the ice drift retrieval near the ice edge and in semi-enclosed seas such as Pechora Sea and Kara Sea is quite limited.



C

Figure 13, continued. c) Ice drift vectors retrieved from two ASAR stripes obtained in the Kara Sea on 26 and 29 May 2005

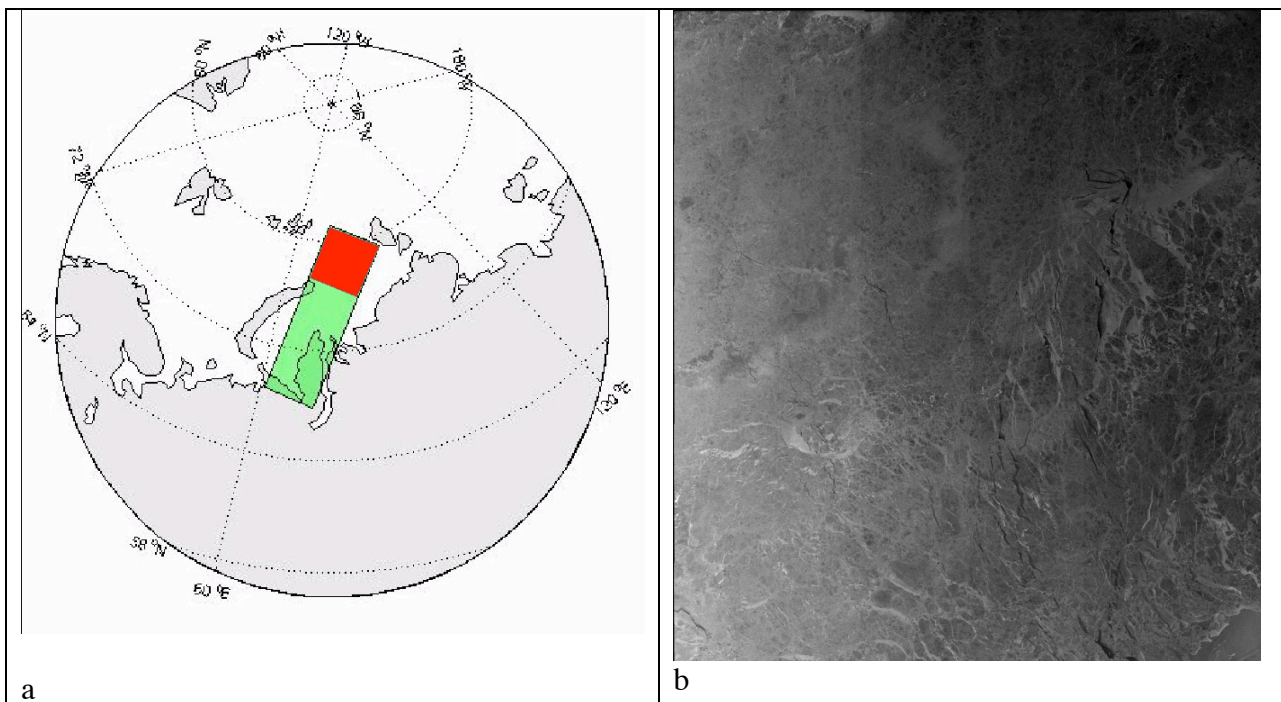


Figure 14. Ice feature detection in SAR imagery. Example from the Northern Kara Sea, location of the image is shown in red (a). b) image showing a number of leads indicated by brighter signature. These were detected and enhanced in Fig. 15 a.

One of the main advantages of SAR images for ice monitoring is the capability to detect and map leads, polynyas, ridges and shear zones. This is very useful information for ice navigation. The frequency of occurrence, size and orientation are properties that can be retrieved from the images by use of various image filtering techniques. The image in Fig. 14 b has been processed to enhance the leads, shear zones and fractures in the ice pack. The results of such analysis is shown in Fig. 15a.

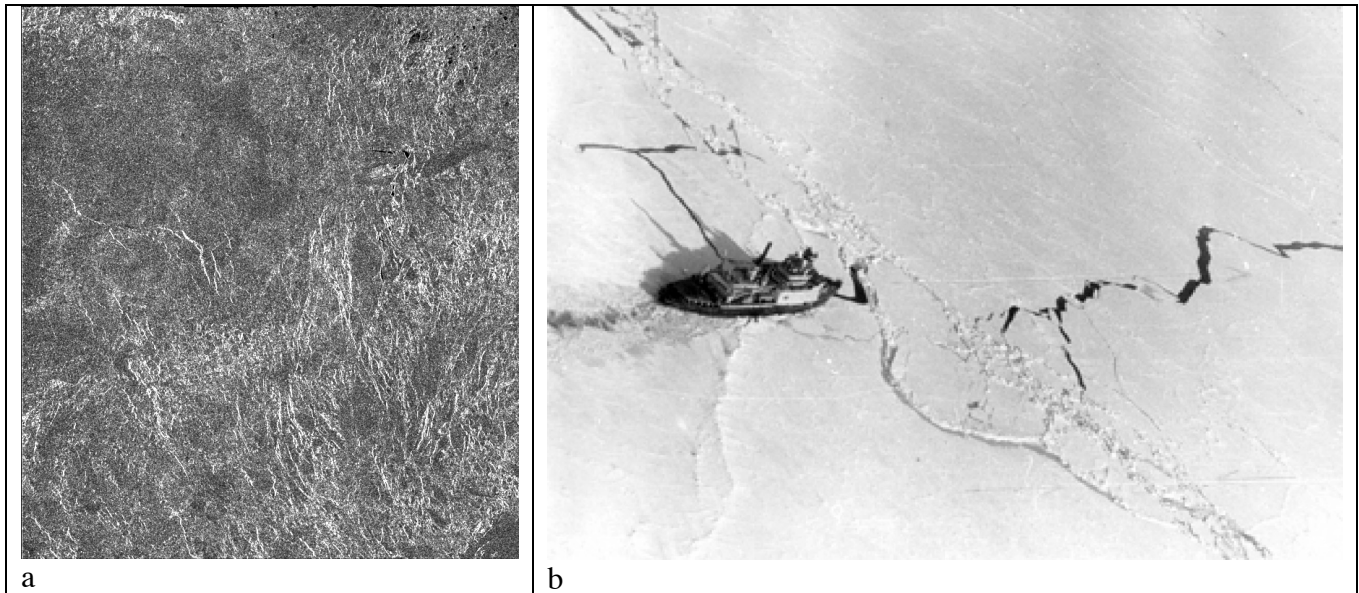


Figure 15. a) SAR image with enhanced ridges, fractures and leads; b) picture of ice navigation perpendicular to the pressure axes (Courtesy, N. Babich, MSCo).

When navigating in ice under pressure, the sailing route should be chosen parallel or close to parallel to ice drift vector and perpendicular to the pressure axis. As a result of pressure, fresh cracks and discontinuities oriented parallel to the axis of pressure are formed in the ice pack. This is shown in a photograph, presented in Figure 15b. For this reason, the orientations of the pressure axes in the ice pack is an important factor in ice navigation. SAR images can contribute with data on the orientation and frequency of such pressure axes.

3. Sea ice signatures in SAR images

3.1 New ice

New ice denotes the first stages in ice formation at the sea surface. The term includes subtypes such as *Frazil*, *Grease*, *Slush* and *Shuga*. *Frazil* and *Grease ice* are usually well-defined in SAR imagery due to the very low backscatter. This ice dampens out the short capillary waves, and thus creates a smooth surface that causes specular reflection of the radar waves. *Grease ice* usually occurs in the ice edge region during cold winter conditions.

Nilas is an elastic ice sheet less than 10 cm thick, bending under pressure. *Nilas* forms from grease ice under quiet conditions with minimal influence of wind and waves. It is subdivided in *Dark*

Nilas (less than 5cm thick) and *Light Nilas* (5 – 10cm thick). SAR backscatter from *Nilas* is usually low because the surface is relatively smooth. As the nilas grow thicker and becomes less elastic, rafting can occur which generates higher backscatter. In SAR images nilas can be misinterpreted as calm water and vice versa. Nilas often occurs in leads and polynyas during the winter season. Examples of nilas are shown in Fig. 16.

3.2 Young ice

Young ice is a further development of new ice and nilas, defined to be in the thickness range from 10 – 30cm. *Young ice* can be subdivided into *Grey ice* (less than 15 cm) and *Grey-White ice* (more than 15cm thick). *Grey ice* is less elastic than nilas and will raft under pressure and break under wave action. *Grey-white* ice buckles to form ridges on its edges from pressure or collisions. Young ice has brighter SAR signatures than grease ice and nilas and usually lower than pancake ice. The brightness increases with more ridges and rafts. Examples are shown in Fig. 17.

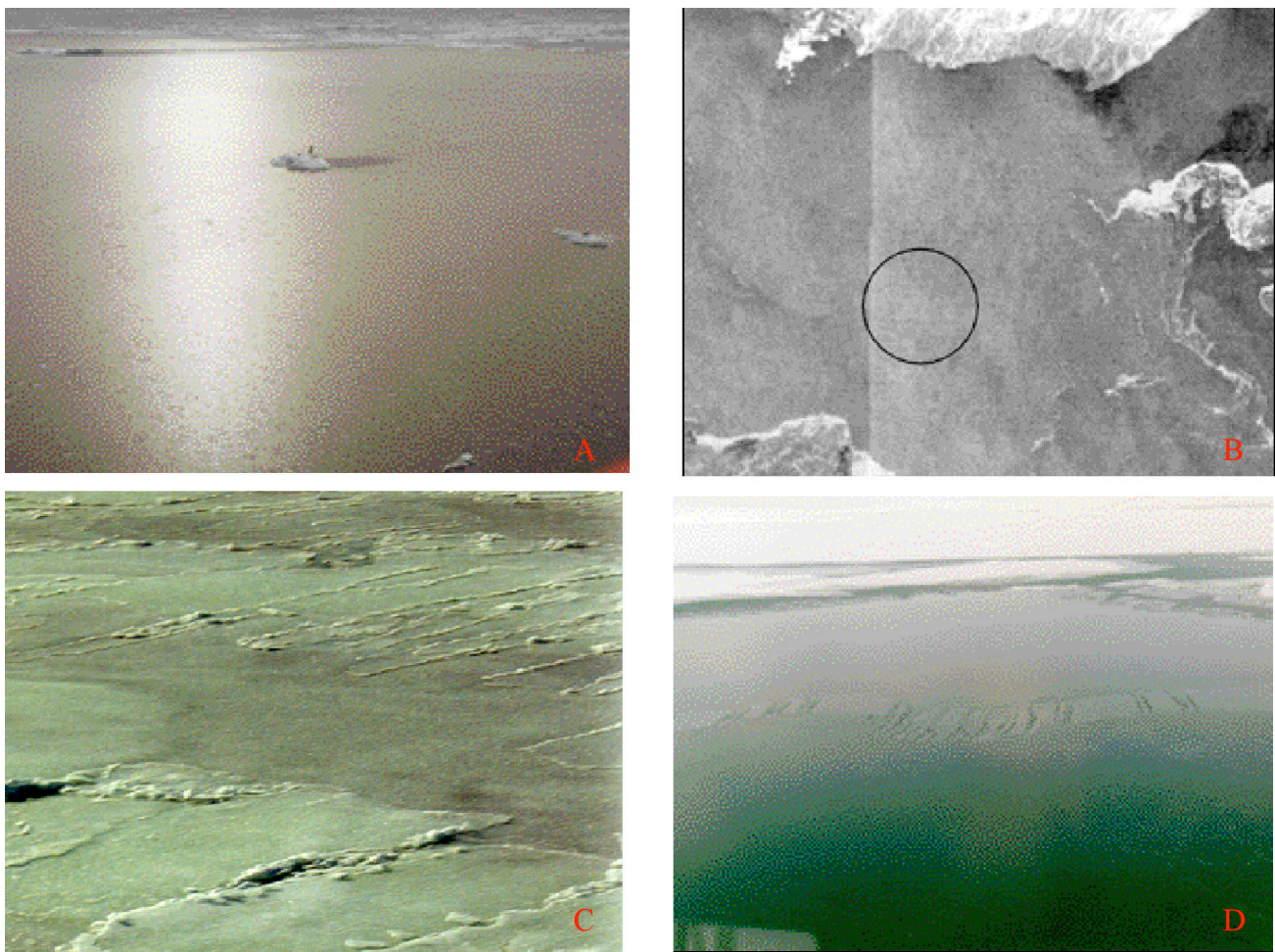


Figure 16. A) Photograph of typical smooth nilas with thicker ice in the background. B) The SAR image showing patches of nilas with uniform and low backscatter. The photograph in A was taken inside the circle with a diameter of about 30 km. The SAR image is a subimage of a RADARSAT ScanSAR image covering the Vilkitsky Strait. Bolshevik Island is seen in the upper part of the image and Cape Cheluskin is seen in the lower left corner. Tongues of old ice are seen as bright bands in the right part of the image. C) Nilas after pressuring, causing formation of rafting and small ridges, taken north of Dikson in April 1998. D) Helicopter picture of nilas with finger-rafting.

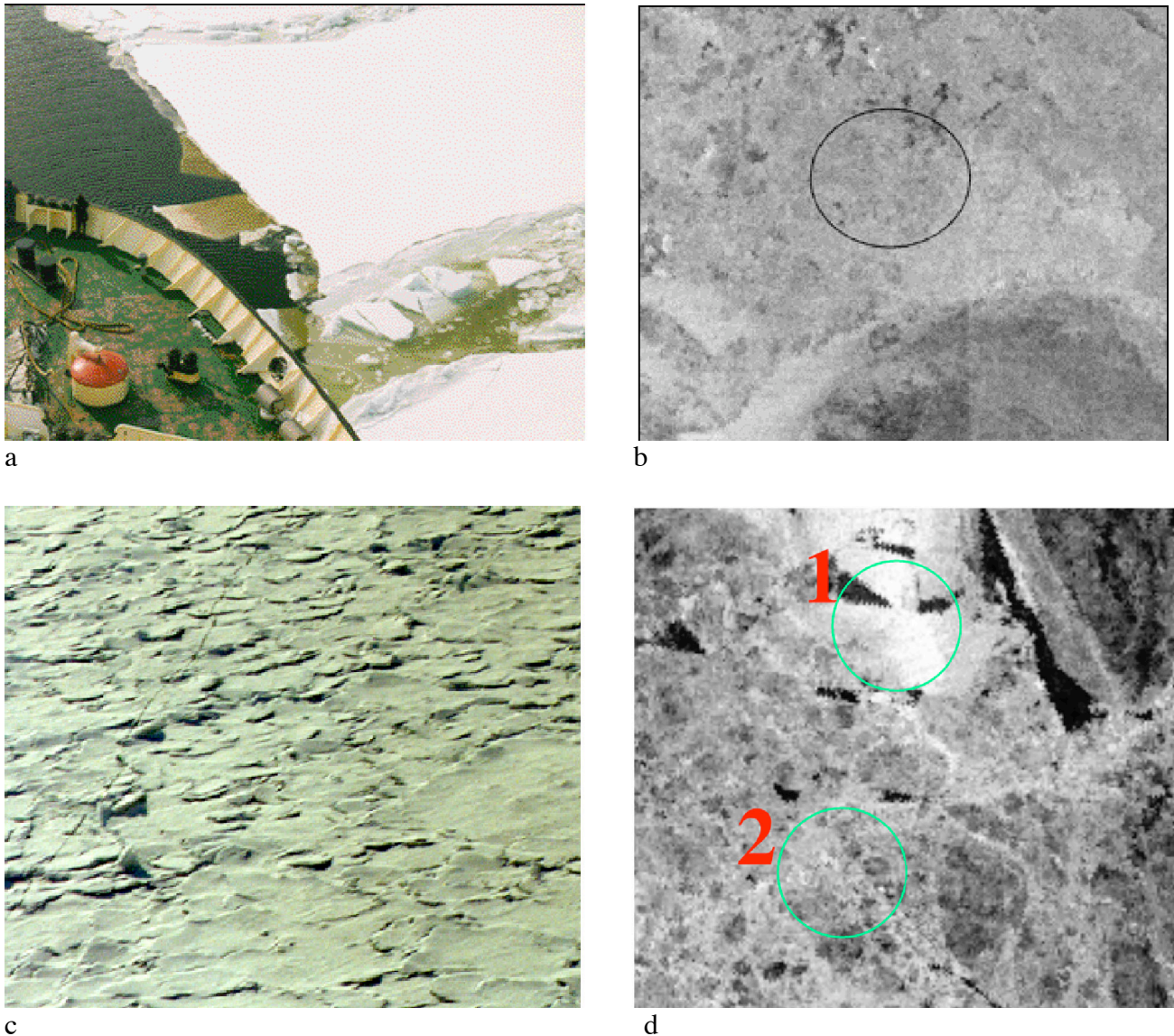


Figure 17. a) Photograph of level young ice bordering an icebreaker channel. b) SAR signature of young ice types with varying deformation and some first-year ice floes. The circle is about 20km in diameter, and positioned NE of Belyy island. c) Photograph grey/white ice with rough surface due to many small edges. This ice gives uniform high SAR backscatter as shown in region 1 of the SAR image in d. The dark areas in the SAR image (d) are nilas. The area in circle 2 shows typical SAR signature of first-year ice with identification of floes.

3.3 First year ice

Firstyear (FY) ice is defined as sea ice formed from water during the present winter, developed from young ice, which is more than 30 cm thick. It is usually divided into subclasses denoted thin (30 - 70 cm), medium (70 - 120 cm) and thick (above 120 cm) FY ice. The SAR backscatter is most sensitive to the surface roughness and floe size, and less sensitive to the thickness. Minimum backscatter is found for level, undeformed FY ice with smooth surface. The backscatter increases with increasing roughness, reaching maximum for ridges and hummocks. In the marginal ice zone,

the backscatter in creases due to smaller floes broken up by wave action. The following examples (Figs 18 and 19) show typical SAR imaging of FY ice with different roughness and floe size.

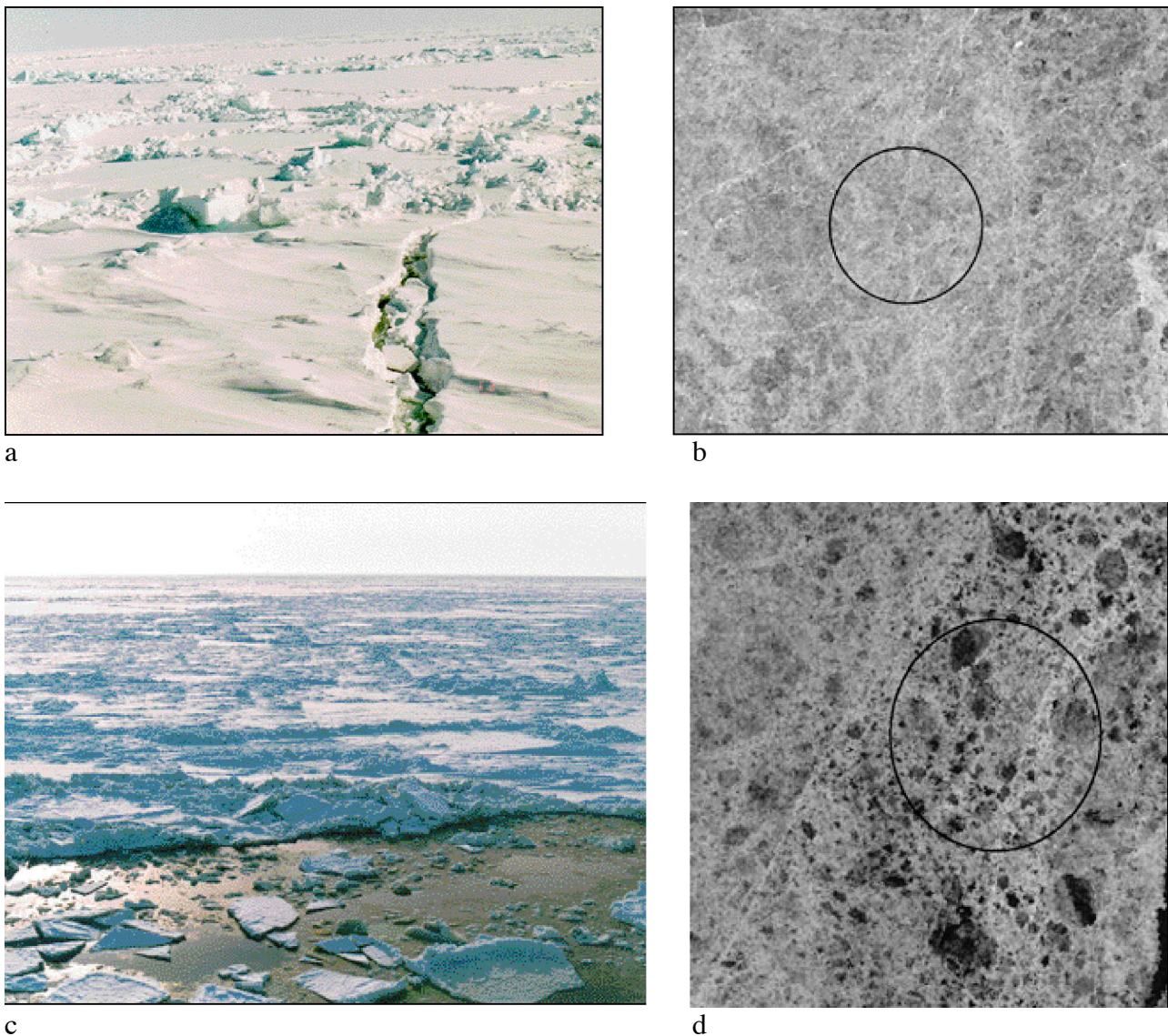
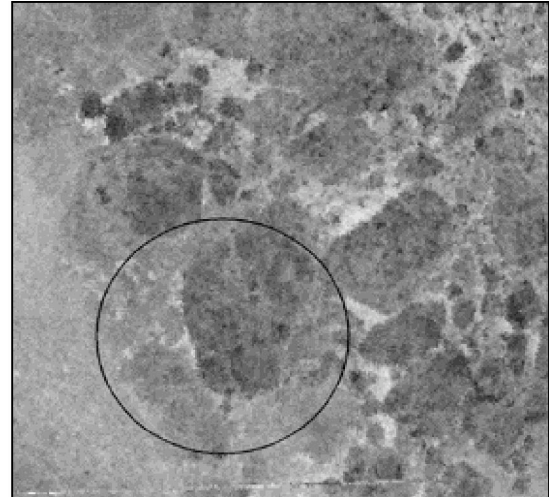


Figure 18. a) Photograph of medium ridged firstyear ice about 1.5m thick, acquired about 150 km west of the Yamal peninsula. The ridges are about 0.5 m high and have typical spacing interval of 100 m. The snow thickness is 15-20 cm. b) Excerpt of a SAR image of the same area acquired two days earlier than the picture in a. The image has a medium backscatter signal typical for moderately ridged firstyear ice. Brighter lines and areas indicate heavier ridging. The diameter of the circle is about 20km. c) Photograph of moderately ridged thin firstyear ice (thickness about 30-40cm), with nilas in the opening in the foreground. d) Excerpt of a SAR image obtained in the same area one day earlier showing both dark areas (undeformed individual floes) and bright lines (ridges and shear zones). This ice is part of the recurring polynya west of the Yamal coast located close to the lower right corner of the image. Picture c was taken within the circle with diameter of about 30 km.



a



b



c



d

Figure 19 a) Medium to thick FY ice west of Dikson, with ridges up to 1.5m. An ice-going vessel is seen in the background. b) Excerpt of a SAR image of the same area acquired 2 days earlier than the photograph in a). Several giant and vast floes with relatively low backscatter can be recognised. The areas with higher backscatter consist presumably of heavily deformed ice or young ice. The photograph is obtained in the medium grey area of the circle with radius 25km. c) The eastern entrance to the Kara Gate with heavily ridged FY ice. Average thickness is more than 2 m and several ridges exceed 4 m in height. This is a very dynamic region and the ice is often heavily deformed. Ice masses are transported between the Kara Sea and the Pechora Sea through the Kara Gate. d) Excerpt of a SAR image of the same area acquired three days earlier than the photograph in c). Ridges similar to those observed in the photo are found in the whole Kara Gate region, giving higher backscatter than less deformed ice in the Kara Sea. The SAR image also shows several very bright features and lines, which can be either open water or very deformed ice, alternatively deformed young ice. Picture c was taken within the circle with diameter of about 30 km.

3.4 Multiyear ice

During the melting season, the thickness and area of the whole Arctic ice pack is reduced. The ice surviving the melt season is called *Old ice*. WMO defines two subtypes of Old ice, *Second-year ice*

and *Multiyear ice*. It is common to use only the term *Multiyear (MY) ice*. This ice is normally thicker, and also less saline than the FY ice formed during the freezing season. This gives MY-ice a significant higher backscatter than FY-ice. Multiyear ice occurs in the northern parts of the Barents and Kara Seas and represent a significant hazard to ice navigation (Figure 20). Multi-year ice can occasionally drift southwards to the Pechora Sea.

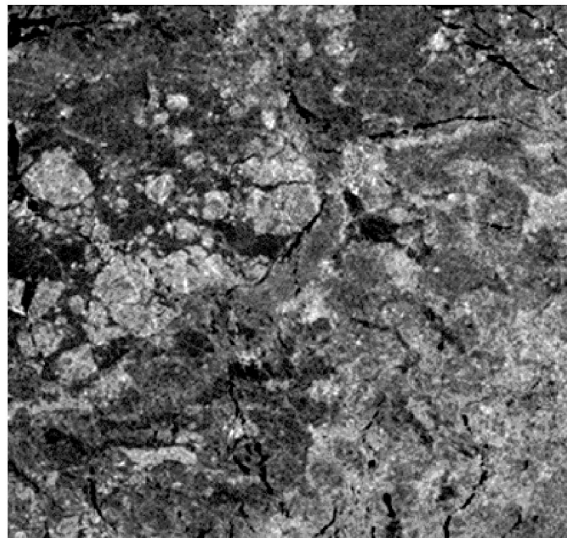
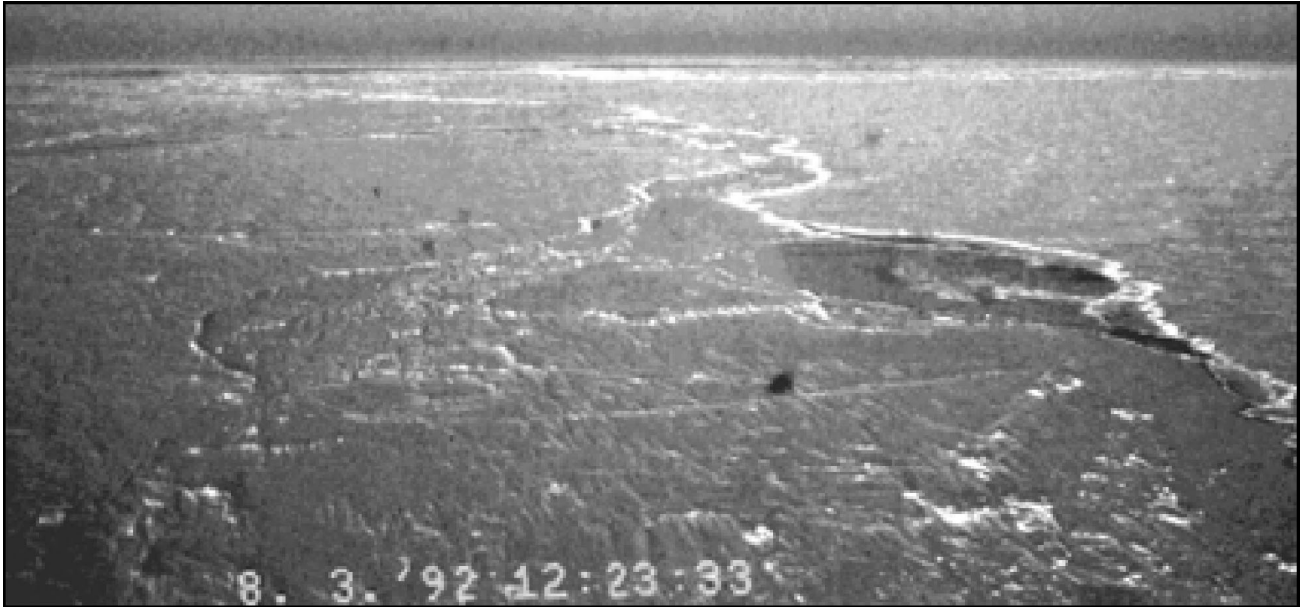


Figure 20. Upper figure: Aerial photograph of part of a 10 km long MY floe observed in the Barents Sea (in the upper right part of the picture). The floe is characterised by a relatively smooth surface, covered by a 0.5m thick layer of snow. The thickness of the floe varies from 2.0 to 4.5m, observed by drilling holes. The ice to the left of the MY floe is a mixture of FY ice and young ice in refrozen leads. Lower figure: Excerpt of a SAR image showing the MY ice floes as brighter patches surrounded by darker FY floes and other thinner ice types. Many of the large MY floes have variable backscatter signatures. The brighter areas in the lower right part of the image are smaller FY floes with similar backscatter as the MY floes. Texture information (shape, pattern, etc.) is needed to separate MY floes from broken-up FY floes.

4. Use of optical satellite images

There are many types of optical satellite images that are useful for observation of sea ice. The most common are NOAA AVHRR, Aqua MODIS, Landsat, SPOT, ASTER and others. The most important characteristic is that the images are limited by cloud and darkness, and therefore most useful on cloud-free days in the spring and summer season in the Arctic. But the images have also advantages compared to SAR, namely that the images can give better resolution of small details (leads, floes, icebergs) especially for high resolution images. The infrared channel can also give data on surface temperatures. These are complementary parameters to what the SAR images can provide. It is therefore useful to combine SAR and optical images in monitoring sea ice on regional and local scale. In the following figures (Fig. 21 – 25) examples of optical images in the Barents and Kara Sea region are presented.

4.1 MODIS images

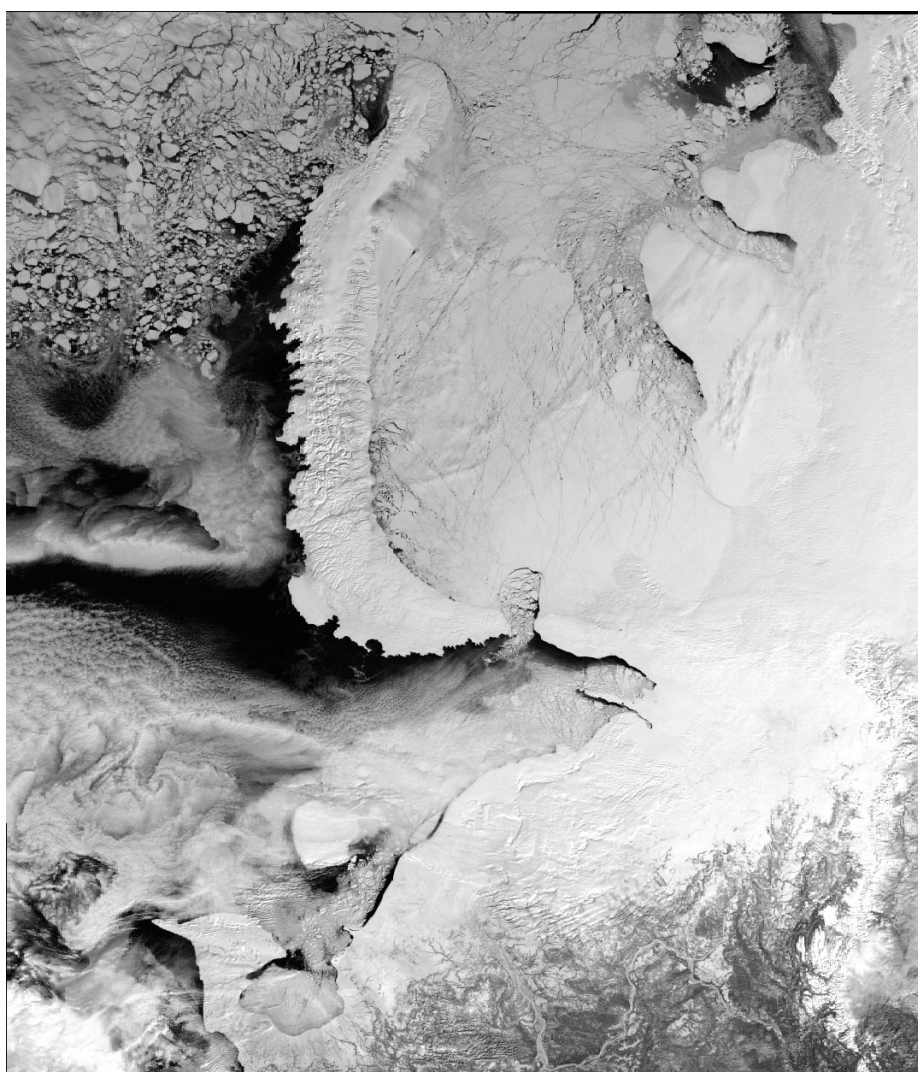


Figure 21. This is an AQUA MODIS image taken on 01 May 2005, with resolution down to 250 m. In general, sea ice is bright in optical images while open ocean appears dark. Clouds also appear as bright features. On cloudfree days such images provide detailed information on ice edge position, ice floes, shear zones, fastice zones, leads and polynyas.

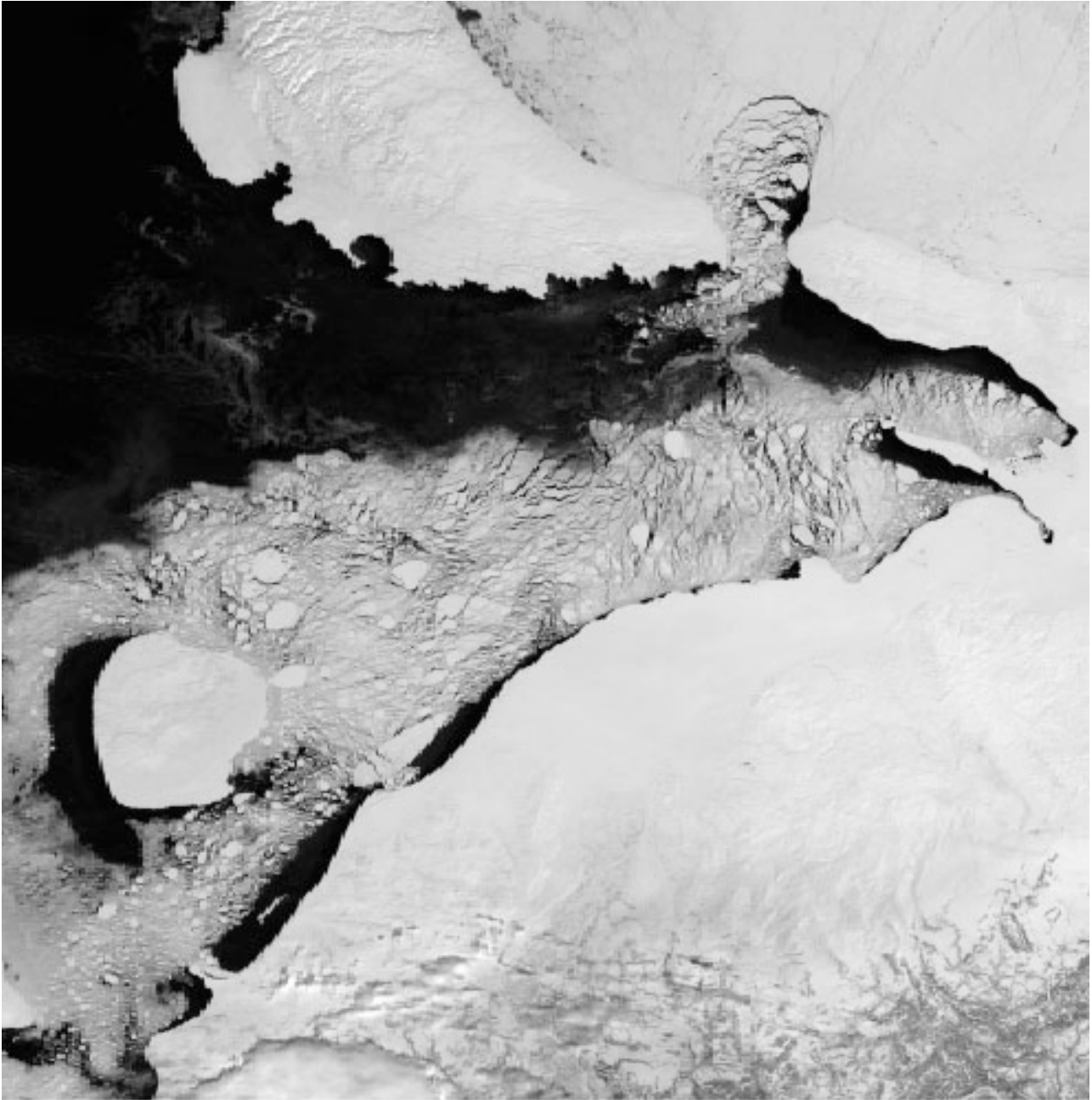


Figure 22. MODIS sub-image from 02 May 2005, zoomed-in on the Pechora Sea and the Kara Gate region. The bright signature from sea ice is in good contrast to the dark signature from open water. This example shows how the ice is pushed away from the coast due to easterly winds. In the Kara Gate it is noteworthy to observe how the easterly winds have started to break up the compact ice cover in the Kara Sea and transport ice floes south-westwards through the strait.

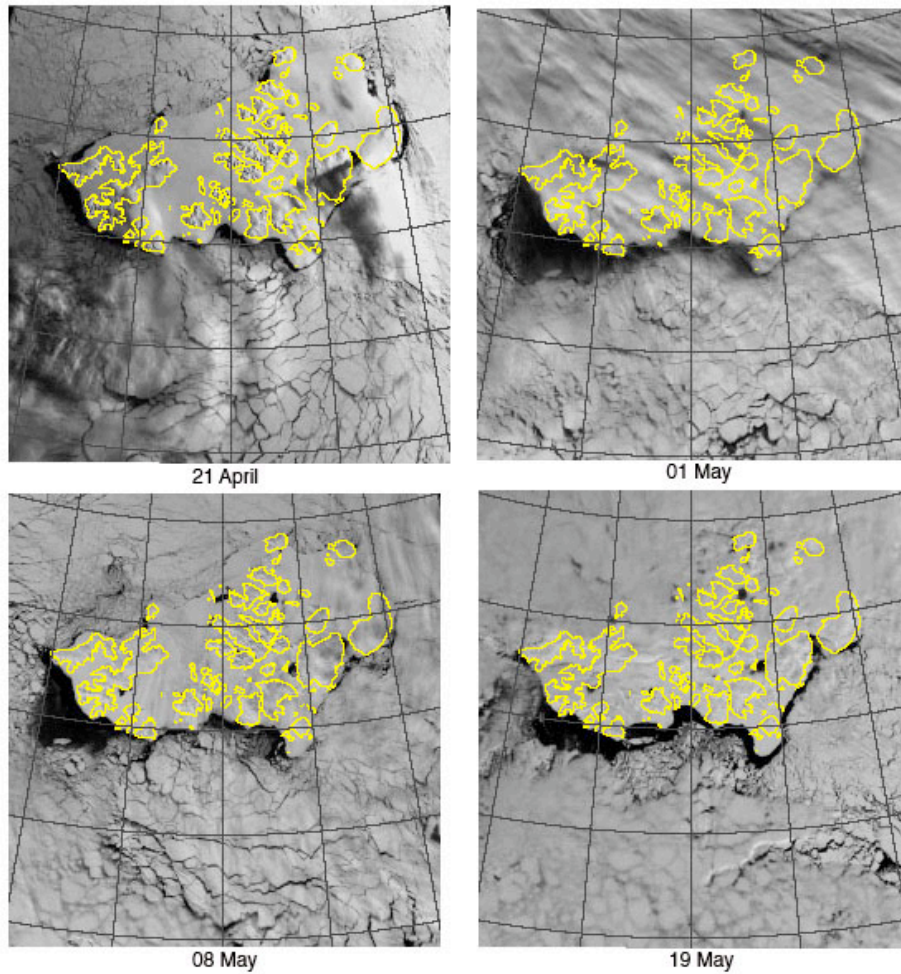


Figure 23. Examples of MODIS images covering the Franz Josef Land area in April – May 2005. The coastline of the islands is superimposed from a database. These images are useful for studying the coastal polynya and sea ice drift south of the archipelago where many icebergs are produced and drift southwards in the Barents Sea. Further studies of icebergs in this region are presented in chapter 4.4.

4.2 Landsat images

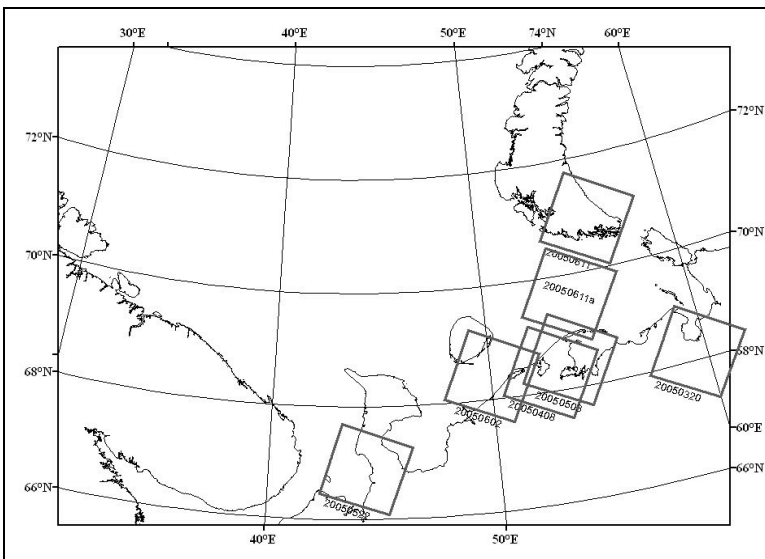


Figure 24. Map of Landsat image location in the Pechora Sea region in spring 2005. The quicklook images showing sea ice are presented in Fig. 25. Landsat images have higher resolution, about 30 m, but cover smaller areas than the MODIS images. Each Landsat scene covers 180 by 180 km. The images are usually obtained over land and in the coastal areas. Landsat images have been obtained for more than 20 years and archives of such images can be used to search for images back to 1982.

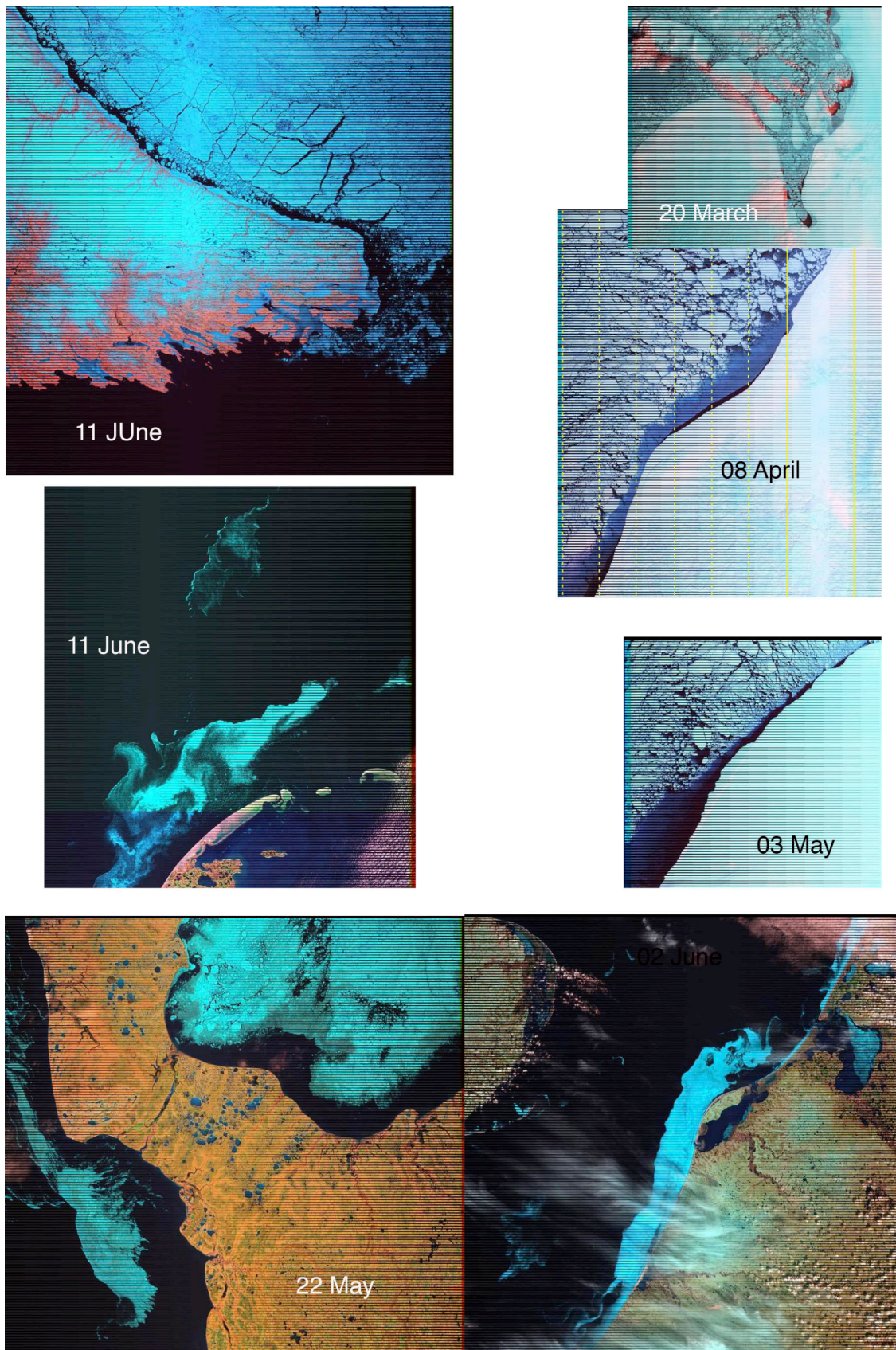


Figure 25 Subset of Landsat quicklook images showing sea ice in the Pechora Sea region in spring 2005.

4.3 Comparison of SAR and Landsat images

The advantage of using a combination of SAR and high-resolution optical satellite images for sea ice observation is illustrated in Fig. 26. This figure shows an excerpt of a Wideswath SAR image from ENVISAT and two Landsat images of the same area with one day interval in June 2005. The advantage of the Landsat images is that they give very good contrast between sea ice and open water. This makes it easy to identify sea ice even if there is only very little ice scattered along the coast, as seen in the lower part of the Fig. 26 b. Furthermore, the Landsat image gives better resolution of ice floes, leads and other smaller scale features of the ice cover compared to the SAR. This can be seen in the area north of the Kara Gate. The SAR images have the main advantage of being independent of cloud and darkness. This means that SAR images can be obtained regularly, year round, which is important for monitoring the dynamics of the sea ice cover. The SAR images have also capability to distinguish between many ice types and ice roughness, as described in chapter 3. SAR images also gives very different backscatter of open water, due to the strong effect of wind speed on the surface roughness. In Fig. 26 a we can clearly see that low backscatter area north of 70N in contrast to the high backscatter near the coast in the Pechora Sea. The backscatter of open water can sometimes be similar to the backscatter of sea ice, which makes ice detection more difficult.

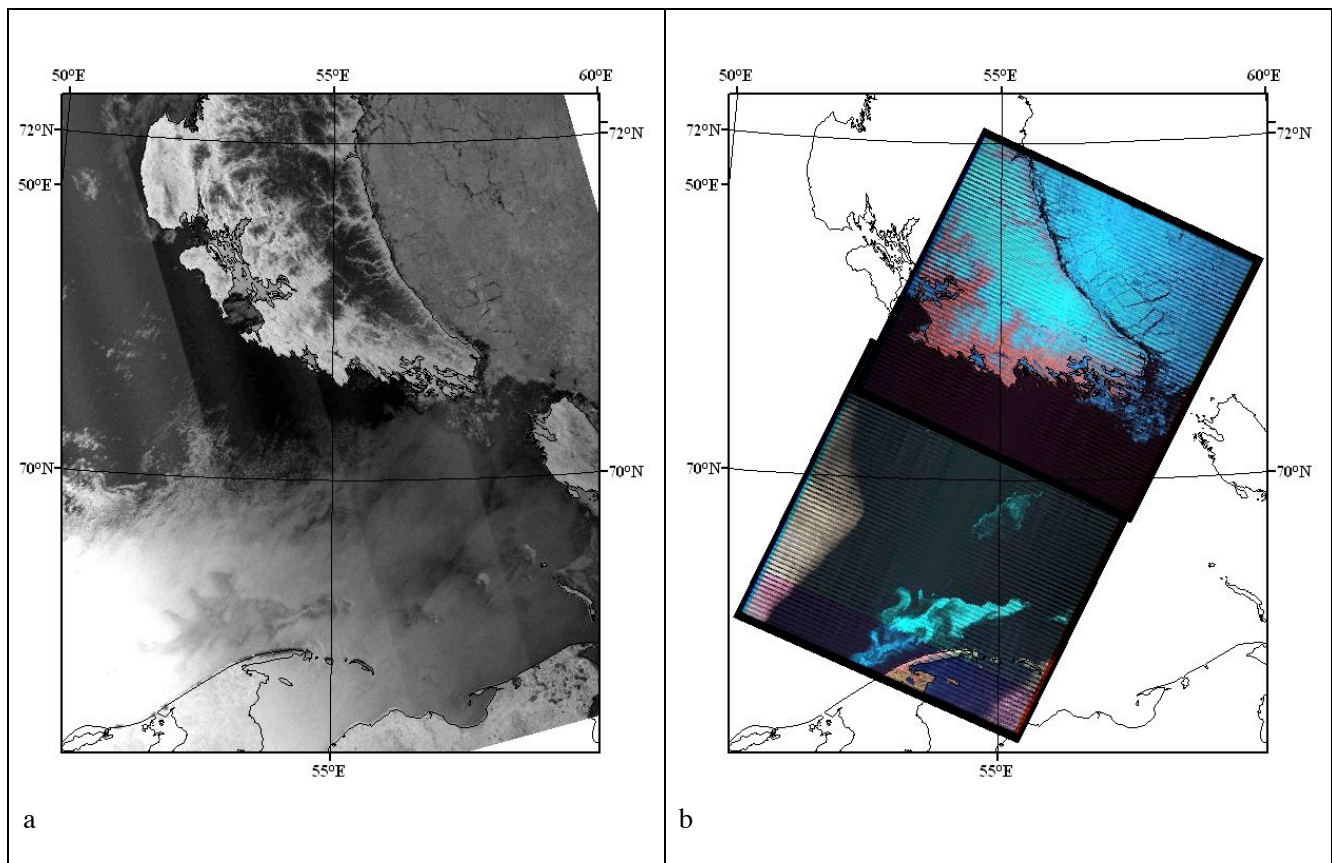


Figure 26. a) ENVISAT ASAR image from 12 June 2005; b) Landsat quicklook images from 11 June 2005.

4.4 ASTER images for iceberg detection

The Advanced Spaceborne Thermal Emission and Reflection Radiometer (ASTER) is an advanced multispectral imager that was launched onboard NASA's Terre spacecraft in December 1999. ASTER has 14 spectral bands from visible to the thermal infrared frequencies. The resolution of the visible and near-infrared (VNIR) images is 15 by 15 m, short infrared images is 30 m, and thermal infrared is 90 m. Each ASTER image covers an area of 60 by 60 km.

In this study we have tested some ASTER images in the Franz Josef Land area for iceberg detection in the period May – June 2005. An overview of the available ASTER quicklook images in this region is shown in Fig. 27. The fastice boundary and the open water polynya on the southern side of the archipelago is similar to what is observed in the MODIS images in Fig. 24. The resolution of the ASTER images is much better than the MODIS images (15 m compared to 250 m), allowing ASTER images to be used in iceberg detection.

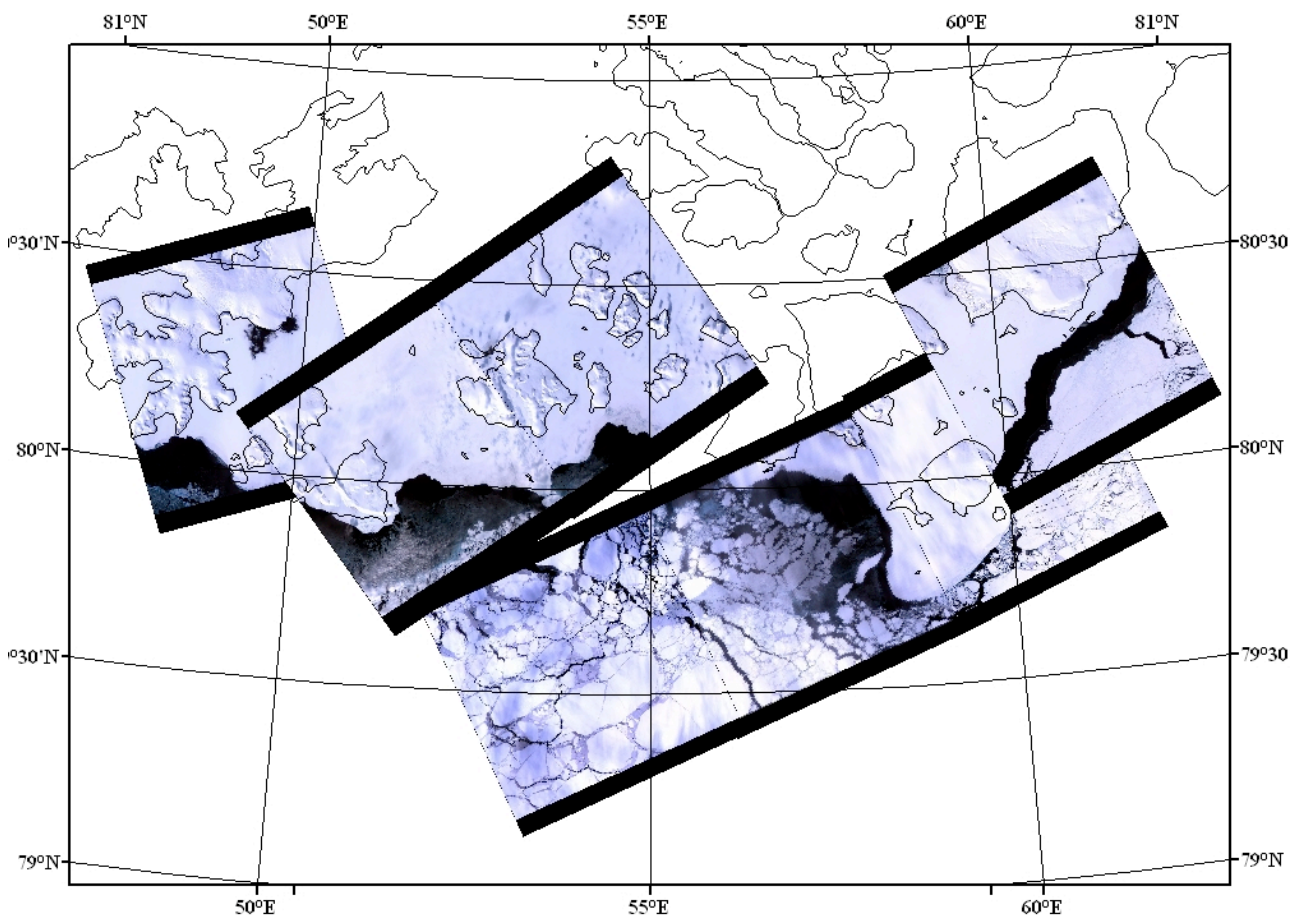


Figure 27. Overview of the ASTER images covering some of the important iceberg calving areas in Franz Josef Land in May- June 2005. One of the images were analysed in full resolution for iceberg detection, as shown in Fig. 28.

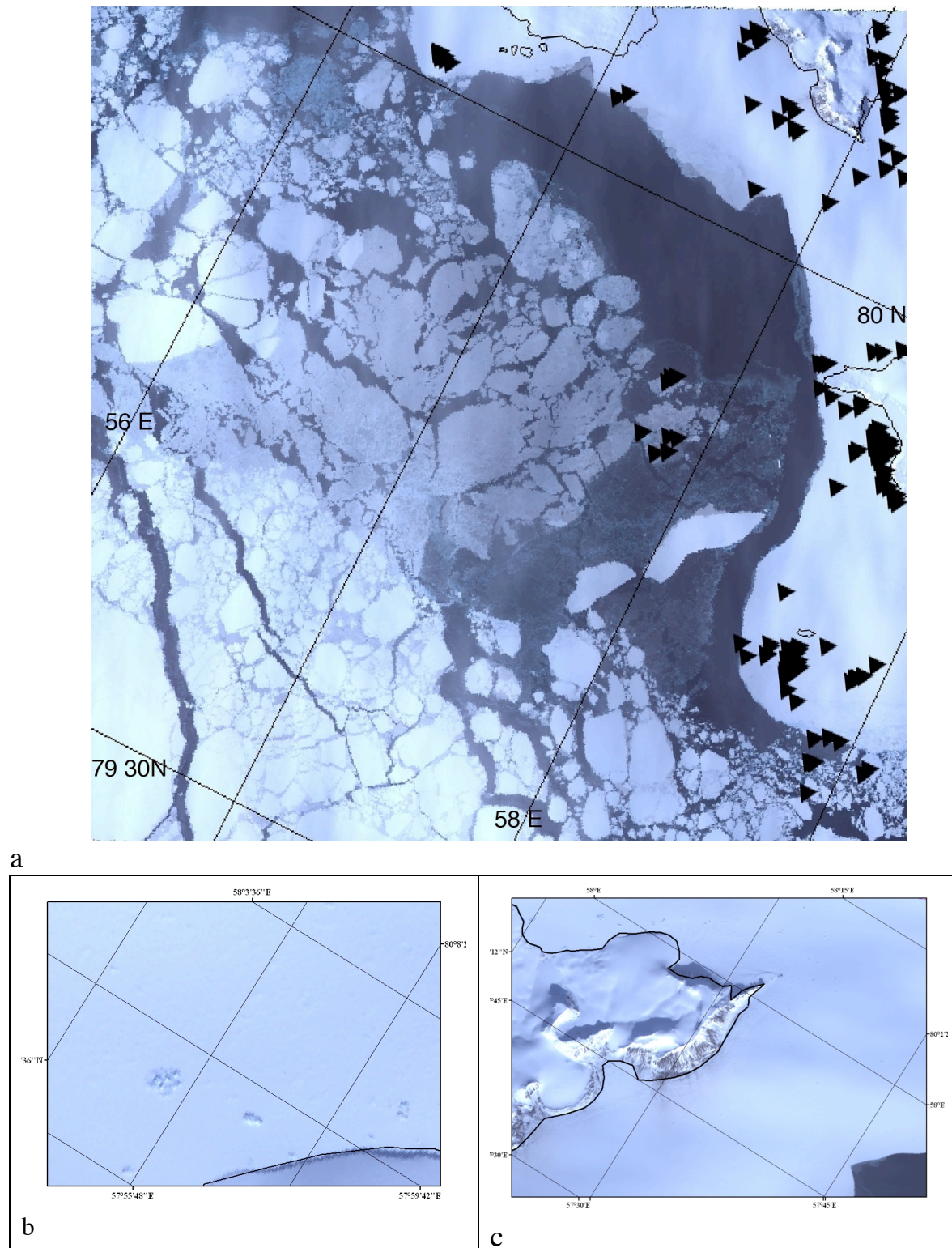


Figure 28. a) ASTER image in full resolution with iceberg locations indicated by triangles. More that 100 icebergs with size above 60 – 80 m were found; b) and c) shows example of zoomed-in areas where icebergs are detected as objects producing a shadow against the uniform bright background. This shadow is caused by the higher elevation of the icebergs compared to the sea ice (see picture on the front page of this report) and the low sun angle.

From previous studies of icebergs in the Barents Sea, it is well known that Franz Josef Land is the most important iceberg producing area, and that the icebergs that originate from this region have a size of typical 100 m or less in horizontal extent. During the Ice Data Acquisition Programme (Kloster and Spring, 1992) and from the Abramov atlas (1996) the following characteristics of icebergs in the Barents have been found:

- Average size: 300 000 tons (90 x 60 x 15m)
- Maximum observed size: 6.2 mill. tons (320 x 270 x 40m)
- Average speed 0.5 knots, maximum 2 knots. Mostly follow southerly current 40E
- Annual iceberg production: Frans Josef Land: 2.3 km³ Novaya Zemlya: 2.0 km³ and Svalbard 1.7 km³

We have not performed any systematic analysis of satellite images in the whole archipelago, but have tested how many icebergs could be detected in one ASTER image, obtained on 09 May (Fig. 28). The results was that 138 icebergs with size above 60 – 80 m were detected. Then we looked at a second image of the same area taken about 5 weeks later. Most of the icebergs were still in the same position, mainly because they were trapped in the landfast ice. However, a few icebergs had disappeared since part of the landfast ice had drifted away. It is assumed that many of the observed icebergs will drift away during the summer and autumn as the landfast ice melts. It is also expected that icebergs near land will stay in the region also during the following winter. The amount of icebergs that are transported out the production areas will depend on the wind and current conditions at the time when the icebergs are drifting freely. Icebergs drifting in the ocean are strongly affected by the tidal currents, as shown in Fig. 29.

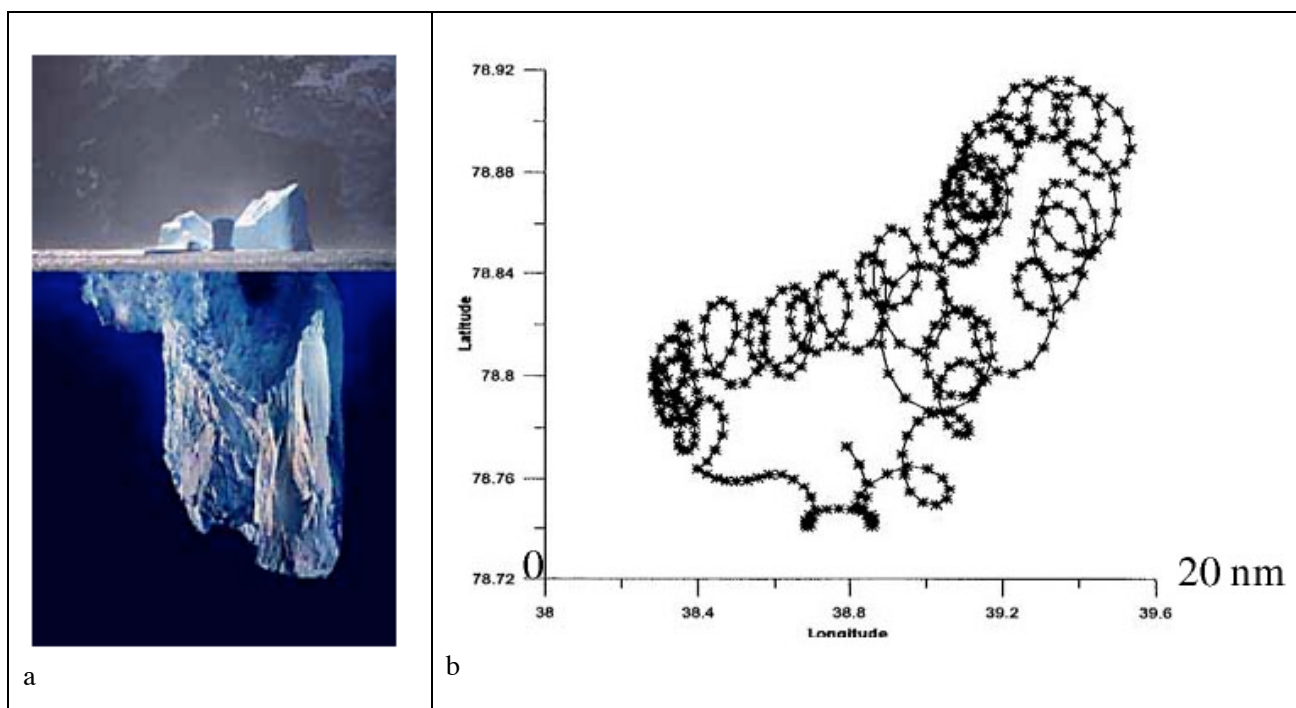


Figure 29. a) Illustration of the draft of an iceberg, indicating the current drag is a very important forcing mechanism for ice drift; b) example of ice drift measurements using ARGOS buoys obtained south of Franz Josef Land in 1990. The semidiurnal tidal current is the dominating component of the current in this region.

5. Ice roughness and thickness from IceSat

5.1 Technical introduction

The Ice, Cloud and land Elevation Satellite (ICESat) was launched in January 2003 with the instrument GLAS (Geoscience Laser Altimeter System) onboard. The GLAS instrument consists of two visual and near-IR lasers for the measurement of surface height directly under the satellite (along the subsatellite line). The main mission objective is to measure volume changes of polar ice sheets and glaciers using a 1064 nm wavelength laser. Among the secondary objectives is the measurement of sea ice roughness and thickness with this laser. The 532 nm wavelength laser is used for atmospheric variables (clouds, aerosols, etc.).

The ICESat orbit has a semimajor axis of 6971 km (that is approximately 610 km height above the Polar Ocean) and an inclination of 94 deg. (that is a retrograde orbit with passes up to about 86 deg N). First the orbit had an 8 days repeat period in order to have a frequent coverage of specific locations for instrument checking. Since the fall of 2003 the orbit has had a 91 days repeat period, in order to cover within 10-15 km of all Earth locations during 3 months. The separation of all one-direction (ascending or descending) tracks available within an 8 days period is $24.2/8 = 3.02$ deg. At 75N lat., this corresponds to 87 km between all the tracks that are made on a weekly basis.

5.2 Examples of laser profile data

Since the sensor is optical, a reasonably clear sky is required to measure the sea ice. The GLAS-data on 14 March 2003 was selected for a first comparison, as it contained a track with clear-sky that was near-coincident (4 hour difference) with an ASAR image over the Barents Sea (Fig 30). Of the other tracks in this period, most were cloud-covered or outside of a suitable near-coincident ASAR image. The GLAS segment that falls within the available ASAR image on 14 March has been extracted from the GLA13 datafile. It is a line of duration 50 sec, between the positions 78.08N, 39.43E and 75.13N, 35.17E that is, over the ice in the Northern Central Barents Sea.

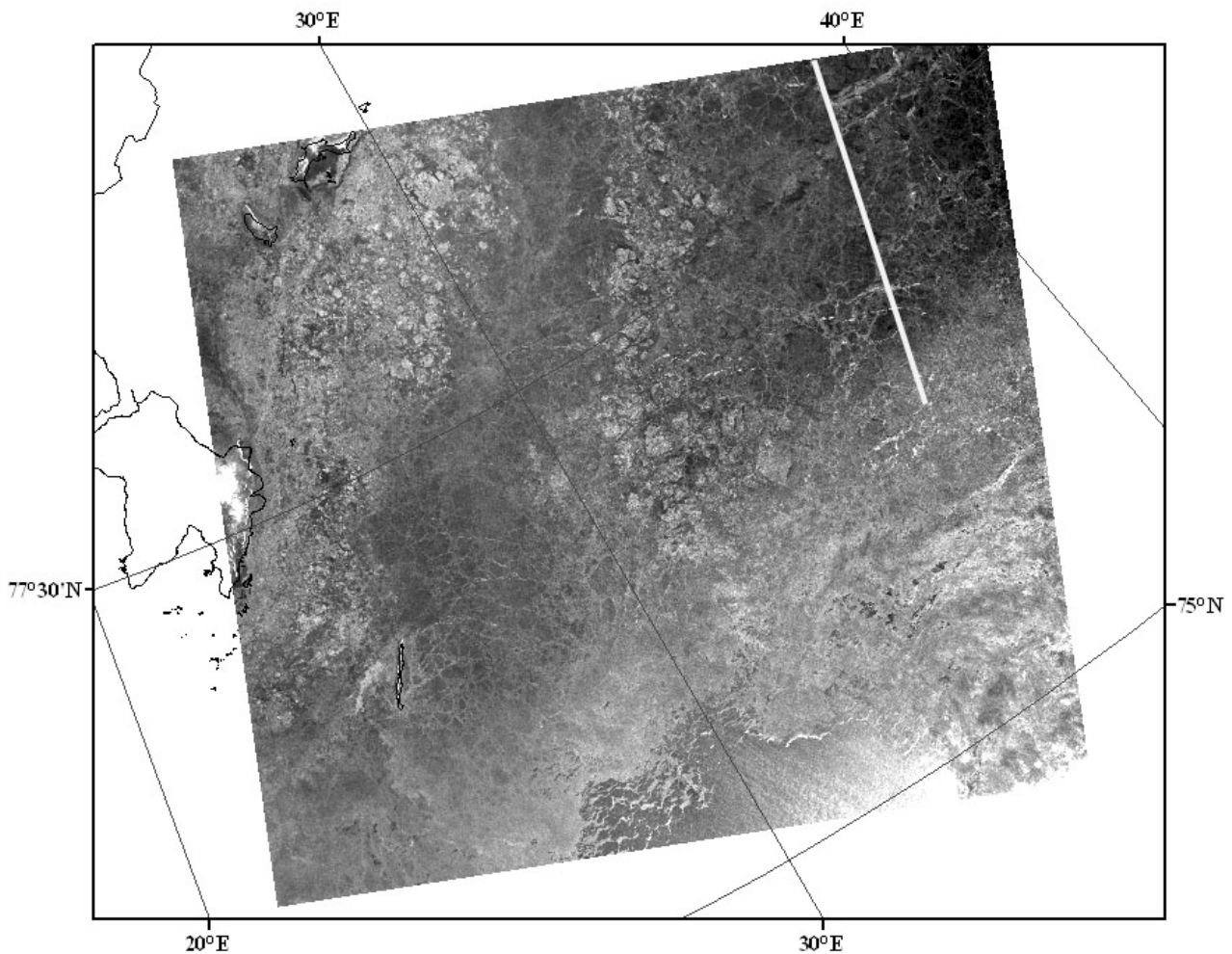
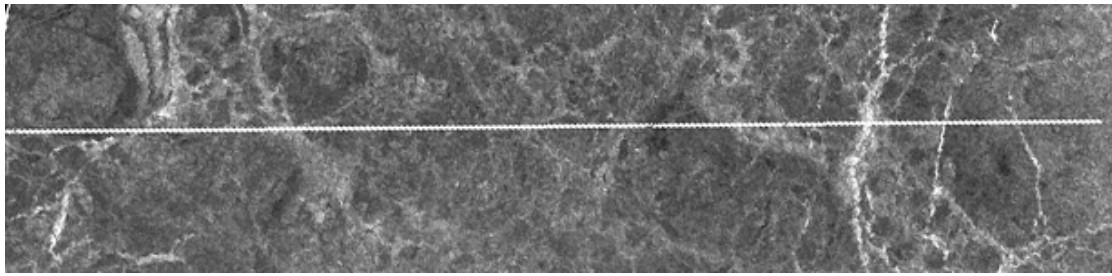


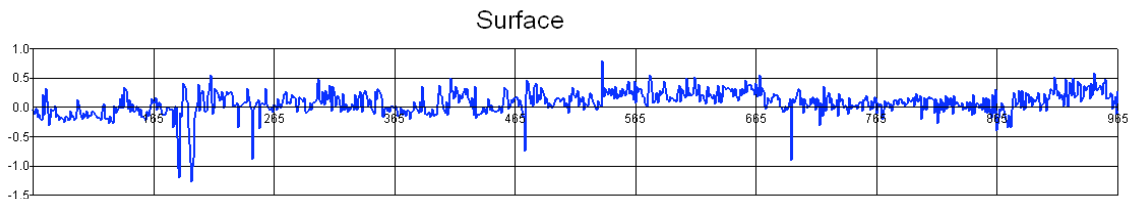
Figure 30. ASAR image in the Barents Sea 14 March 2003 with the IceSat laser profile superimposed as the white line. The profile extends out in open water, but the data in the ice edge region has been omitted due to cloud cover.

Processing of profiles of surface height, reflection and roughness is made as function of position (or time) along the ground track. The two first profiles are presented in Fig. 31 b and c. The actual sea surface is not the geoid, so the zero line of the height profile must be adjusted to show the real freeboard, that is the measured surface height above the water. This adjustment can be made by assuming that the lowest heights on the curve corresponds to open leads or very thin ice with zero height. The variation of the surface height curve is generally within half a meter. This corresponds roughly to ice thicknesses up to max 3 –4 m, assuming a snow-thickness of about 20 cm on the thicker ice.

The profile of surface reflectance is plotted in Fig. 31 c. It is generally high (about 70%) corresponding to snow cover on thick ice. A few peaks above 100% or below 0% are probably caused by an over-steering of sensor sensitivity for rapid variations. Sections with low surface reflection is expected to correspond to leads with thin, snowfree ice or water. This is also seen in some places along the profile, although this profile does not seem to cross any wide leads.



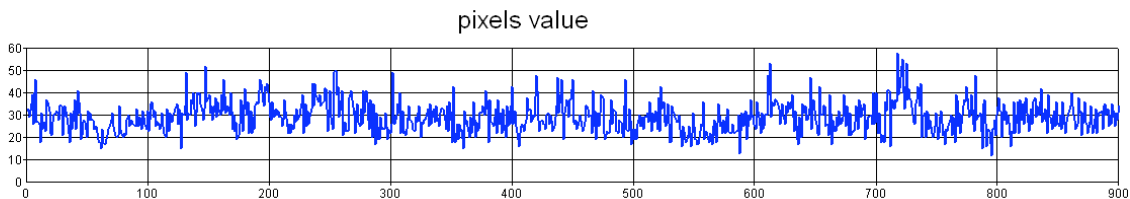
a



b



c



d

Figure 31. a) Subset of the ASAR image from 14 March with IceSat track superimposed; b) surface elevation profile (in m); c) surface reflection profile; and d) SAR pixel value profile.

On the image of 14 March that is taken 4 hours earlier than the GLAS line, it is seen that the lidar track crosses several long, narrow and bright areas. This stronger radar signal are generally caused by rough ice in earlier leads (thinner ice that has been rafted and/or ridged by ice convergence). The ice in these areas may be both thinner (rafted ice less than 30cm thick) and thicker (ridged ice more than 30cm thick) than the surrounding smoother FY-ice of about 1 –2 m general thickness.

Comparing the ASAR backscatter with the GLAS surface height indicate some correlation (as lower height for brighter backscatter). But the correlation is weak since none of these brighter radar areas are caused by sufficiently new and wide leads to give a good correspondence to the GLAS height signal. Further analysis of GLAS-lines that are crossing wider and newer leads are expected to show a better correspondence (Kwok 2004). Examples of IceSat data analysis and comparison with SAR are shown in Fig. 32.

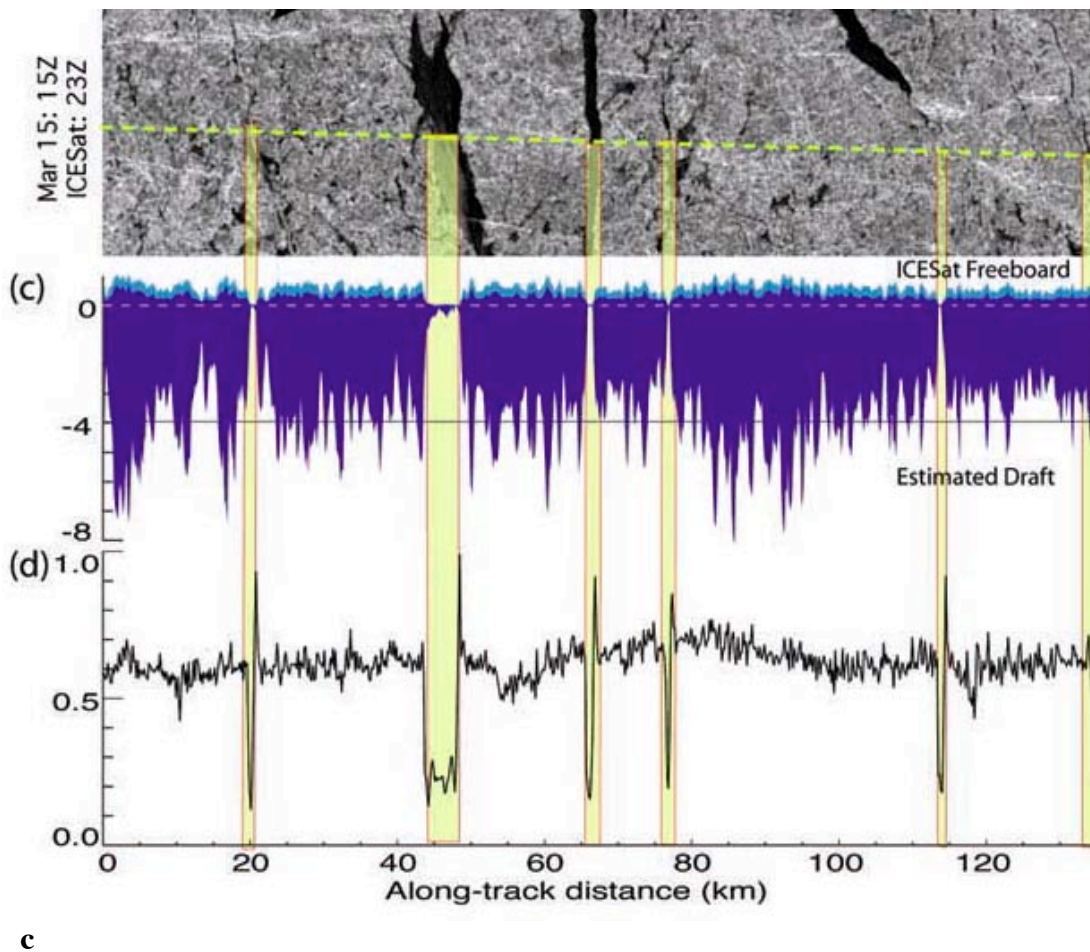
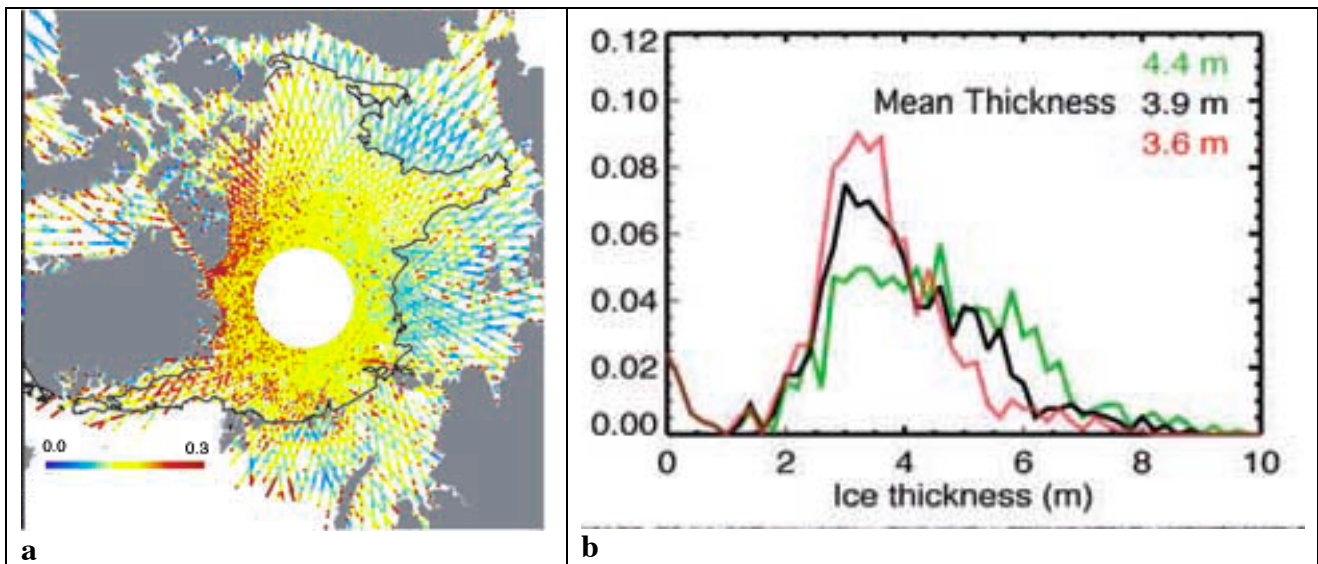


Figure 32. a) Surface roughness from IceSat altimeter, calculated at a 10 km length scale from elevation data (colour coded profiles) and the edge of the multiyear ice derived from scatterometer; b) examples of ice thickness probability density function for the area north of Ellesmere Island, c) profile of laser data (freeboard and estimated thickness) collocated with a SAR image from 15 march 2003 (Kwok, 2004).

6. Conclusions and recommendation for further work

In this report we have collected and analysed several types of satellite data that can quantify some of the sea ice and iceberg properties that are important for planning of Statoil's activities in the Barents and Kara Sea region. Daily passive microwave data are useful for mapping ice concentration and ice extent on regional scale in order to follow the ice edge and ice drift. These parameters are needed as input data in sea ice and iceberg drift models. At present daily, near real-time data are assimilated in the TOPAZ ice forecasting model, and will be used also in the Barents Sea model.

For detailed mapping of ice types, ice concentration, ice drift, ice convergence/divergence, multiyear floes, ridges and leads SAR images have been collected for most of the study period in 2005. Several examples of analysis of the SAR images, including ice drift retrieval, have been shown. From February SAR widewidth mosaics have been made more or less regularly throughout the year in the Kara Sea region. This demonstrates how ice mapping can be improved compared to the standard ice charts delivered by the national ice services. 2005 is the first year when such SAR mosaics are produced in the Kara Sea region. Selected images have been used to support Murmansk Shipping Company's icebreakers during voyages between Murmansk and Dikson. Images have been geolocated and radiometrically corrected before they were transmitted to the icebreaker operational headquarter. The icebreakers have provided in situ reports of the sea ice as they traveled through the areas covered by SAR. This is a useful method to verify the analysis of the SAR images. The detailed information about leads and ridge areas are examples of important ice information needed to operate ships in ice. Vessel which will operate in sea ice in the future need to have SAR-based information as often as possible.

SAR is the most important space instrument for mapping sea ice properties in support of ice operations and navigation. The interpretation of ice properties and processes in the SAR images have been reviewed, because this represent the state-of-art knowledge of SAR ice signatures built up over many years. Use of SAR images for retrieval of ice information will be further developed in the coming years, since new SAR satellites are planned with higher resolution, multipolarisation and both C- and L-band. This will improve the possibility to extract specific features such as ridges, ice classes and ice-water discrimination.

Use of optical satellites to map sea ice has been demonstrated, and the pros and cons of using optical versus SAR for ice mapping has been discussed. The conclusion is that SAR is the most reliable source because it gives good quality data year round independent of cloud and light conditions. Optical data will have an important role as supplement because it provides complementary information. For iceberg detection, high resolution optical images have been demonstrated in the Franz Josef Land area. In one ASTER image more that 100 icebergs were found embedded in the fastice surrounding the archipelago in May 2005. For monitoring of iceberg production and iceberg drift, it is useful to have a systematic scheme for optical as well as SAR images with sufficient high resolution. Such monitoring system should use images with resolution of about 10 m or better. The iceberg monitoring scheme should be combined with the iceberg forecasting model and with drift data from ARGOS or GPS buoys.

Finally, examples of data from IceSat, using laser altimeter, have been presented. CryoSat, which was launched on 08 October 2005, failed and did not reach into its orbit. In the near future other methods for ice thickness need to be used. Further use of satellite data for sea ice and iceberg monitoring will be adapted to the specific needs of the offshore operations and transportation in the region.

The use of SAR data for monitoring sea ice should be continued to build up a good data set for sea ice analysis and estimation of ice drift, mapping of leads, polynyas, shear zones and ridges. The ice drift data will be used to test the Barents Sea model including the iceberg drift model. The SAR analysis will also be used for support to ice operations and ice navigation. Further analysis of ASTER images, supported by high resolution SAR images should be done, with focus on the calving areas in Franz Josef Land and Novaya Zemlya. This will be useful input to modeling the drift trajectories of icebergs. Finally, schemes for using satellite data as input to ice management on local scale should be investigated.

7. References

- Abramov, V. Atlas of Arctic Icebergs. Backbone Publishing Company, 1996, 70 pp.
- Alexandrov, V. Yu., S. Sandven, O. M. Johannessen, Ø. Dalen and L. H. Pettersson. Winter navigation in the Northern Sea Route. *Polar Record*, Vol. 36 (199), 333-342, 2000.
- Johannessen, O.M., S. Sandven, L.H. Pettersson, M. Miles, K. Kloster, V.V. Melentyev, L.P. Bobylev and K. Ya Kondratyev (1996) Near-realtime sea ice monitoring in the Northern Sea Route using ERS-1 SAR and DMSP SSM/I microwave data, *Acta Astronautica*, **38**, 0094-5765, Nos. 4-8, pp. 457-465.
- Johannessen, O. M., A. M. Volkov, L. P. Bobylev, V. D. Grischenko, S. Sandven, L. H. Pettersson, V. V. Melentyev, V. Asmus, O. E. Milekhin, V. A. Krovotyntsev, V. G. Smirnov, V. Yu. Alexandrov, G. Duchossois, V. Kozlov, G. Kohlhammer and G. Solaas. ICEWATCH - Real-time sea ice monitoring of the Northern Sea Route using satellite radar (a Cooperative Earth Observation Project between the Russian and European Space Agencies). *Earth Observation and Remote Sensing*, Vol. 16, No. 2, 257 – 268, 2000.
- Johannessen, O. M. and S. Sandven. Monitoring of the Arctic Ocean. In *Operational Oceanography, Implementation at the European and Regional Scales*. Proceedings from the Second international Conference on EuroGOOS, 11 – 13 March 1999, Rome, Italy, pp. 165 – 177, Elsevier Oceanography Series, 66, 2002.
- Johannessen O. M., V. Yu Alexandrov, I. Ye. Frolov, S. Sandven, M. Miles, L. P. Bobylev, L. H. Pettersson, V. G. Smirnov and E. U. Mironov. *Polar Seas Oceanography, Remote Sensing of Sea ice in the Northern Sea Route: Studies and Applications*. Praxis Springer, in press 2005.
- Kloster, K. and W. Spring, Iceberg and glacier mapping using satellite optical imagery during the sea ice data acquisition programme (IDAP). *Proceedings of POAC 1993*, pp. 413 – 424.
- Kwok, R., 2004. ICESat observations of Arctic sea ice: A first look. *Geophys. Res. Lett.*, 31,
- Mulherin, N.D., The Northern Sea Route. Its development and evolving state operations in the 1990s. US Army Engineer District, Alaska. CRREL Report 96-3, 1996.
- Pettersson, L. H., S. Sandven, Ø. Dalen, V. V. Melentyev and N. I. Babich (1999) Satellite radar ice monitoring for ice navigation of the ARCDEV tanker convoy in the Kara Sea. *Proceedings of The 15th International Conference on Port and Ocean Engineering under Arctic Conditions*, Helsinki, Finland, August 23 – 27, 1999, pp. 141 – 153.

Sandven, S., Ø. Dalen, M. Lundhaug, K. Kloster, V.Y. Alexandrov, and L. V. Zaitsev (2001) Sea ice investigations in the Laptev Sea area in late summer using SAR data. *Canadian Journal of Remote Sensing*, vol. 27, no. 5, 502 – 516.